Exploring Epilepsy: An Investigation of Heterogeneity on Seizure-prone Networks of Neurons Through Computational Modelling

Written By:

Paul Foley

Supervised By:

Jérémie Lefebvre

Thesis submitted in partial fulfillment of the requirements for the Master of Physics degree

Department of Physics

University of Ottawa

Table of Contents

Declaration of Work

I declare that all work in this thesis, titled “Exploring Epilepsy: An Investigation of Heterogeneity on Seizure-prone Networks of Neurons Through Computational Modelling”, has been completed by Paul Foley under the Department of Physics at the University of Ottawa. The information taken from literature has been fully referenced in text with full references provided. All figures used from ulterior sources have been used in concordance with the appropriate copyrights. No section of this thesis has been previously presented for another degree or diploma.

Paul Foley	26/08/2022
Name	Date

Abstract

Epilepsy is a neural disease characterized by rhythmic synchronous firing of neurons, also called seizures. These seizures can be modelled as oscillations of voltage input into neighboring neural regions. In this thesis we put forward a leaky integrate-and-fire network model to investigate how seizure-like inputs interact with heterogeneity. We find that heterogeneity supresses oscillatory behaviour of the network, linearizing the system, with large decreases seen in both resonant and higher-order harmonics. While some frequencies do not follow this trend, heterogeneity is shown to decorrelate excitatory-inhibitory networks, promoting asynchronous firing.

Acknowledgements

While this thesis tells the story of our research, I learnt a lot more throughout the course of this Master's. Countless Krembil Computational Neuroscience and University of Ottawa meetings have introduced me to concepts within neuroscience, both computationally and biologically; the transition from not knowing what an action potential was to being someone who is familiar with the basics of various lab techniques and deep learning methods would not have been possible without the wonderful people at both establishments. I also had the opportunity to present a poster at the Canadian Neuroscience Meeting, which introduced me to many people outside the world of computational neuroscience and showed me just how wide reaching the questions in neuroscience are. While countless people have helped me over the last two years, I want to give a special thank you to Jérémie Lefebvre, his lab, Scott Rich, and everyone at KCN; without them none of this thesis would have been possible.

List of Figures

List of Tables

Chapter 1

Background

§1.0: Chapter Summary

In this chapter we put forward the basic biological properties of neurons and the processes involved in sending and receiving signals to provide a general map of what our work involves. We follow this discussion with an introduction to two different models, these being the Hodgkin-Huxley and integrate-and-fire, where we talk about the general features, benefits, and detriments of using each model to paint a picture of which should be chosen depending on research desires. We define the terms used when analyzing results; specifically, we put forward the firing rate, spectral power, synchrony, and synchrony measure as important features of results. We conclude this chapter by proposing a region of interest for our research in the form of seizures and describe what is seen when these occur; we also describe epilepsy and some biophysical features of epileptic tissue.

§1.1: Neurophysiology of Neurons

Neurons are the primary cells which the brain uses to send and receive information [1]. While there are many varieties of neurons, each consist of three main components: the dendrites, soma, and axon. The dendrites act as the receiver for a neuron, and as a lot of information may be received at a given time there are multiple branches of dendrites. The soma localizes all received information. If certain conditions are met, which are described in more detail in §1.2, information is emitted via the axon. Two morphologically different neurons are shown in Figure 1.

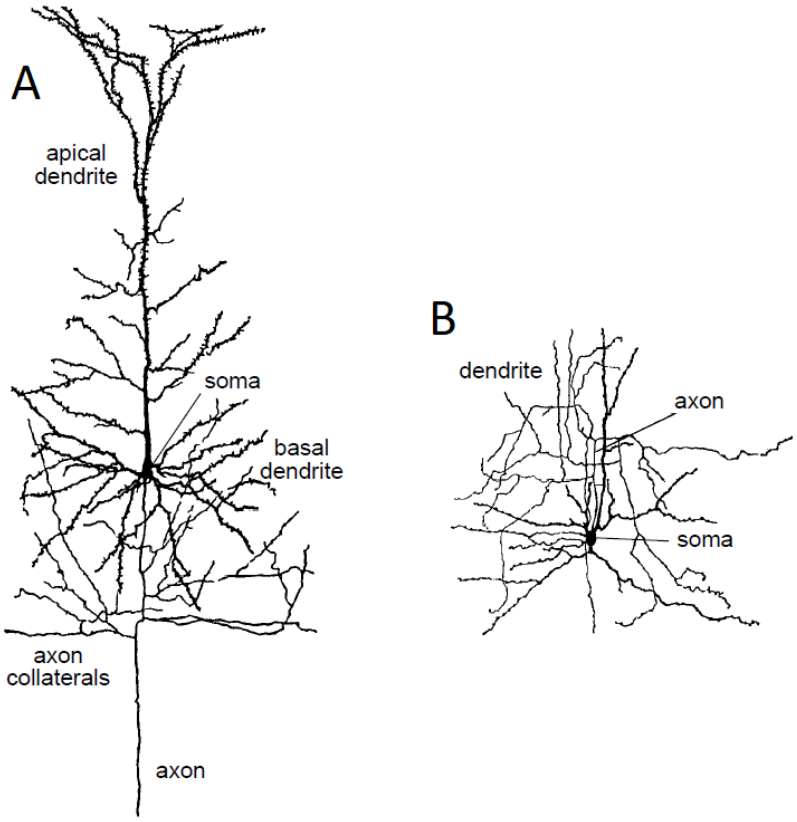

Figure 1: Diagrams of a cortical pyramidal cell (A) and a stellate cell (B) which are the most common excitatory and inhibitory cells in the cerebral cortex respectively. While the fundamental structures that compose the neuron are the same, the morphology they take are quite different. Diagram is taken with permission from [1].

§1.2: Biophysics of Neuronal Excitability

Voltage, or equivalently potential difference, describes the work required to move a charge from one point to another [20]. When discussing neurons we refer to the membrane potential to describe the voltage between the inside and outside of the cell, across the cell membrane. Neurons usually have an equilibrium voltage around -70 mV, but fluctuations naturally arise [19].

The membrane potential stems from ionic concentrations inside and outside the cell [44]. The outside of the cell – extracellular – is considered to have normal ionic levels. The inside of the cell – intracellular – has lower levels of Na^+ and Cl^- ions and an excess of K^+ and negative molecules denoted A^-. Unlike individual ions, A^- are too large to pass through the membrane. Ionic concentration imbalances make neuronal excitability possible. This means that while the ions may theoretically come to a concentration equilibrium, it would produce a net negative intracellular charge which would attract positive ions. A neuron is considered in equilibrium when it reaches a steady state balance between ionic concentrations and membrane potentials that is maintained via energy expenditure.

The potential difference required to achieve equilibrium, for each ion, is called the Nernst potential – E_{Ion} – defined by:

$$E_{Ion} = \frac{RT}{zF} \ln\left(\frac{[Ion]_{out}}{[Ion]_{in}}\right). \quad (1)$$

Extracellular and intracellular concentrations of the ions are denoted by the square brackets. Other parameters are the universal gas constant – R –, the temperature – T –, Faraday's constant – F –, and the valence – z – of the ion. The cell is in thermal equilibrium with its surroundings. The Nernst potential returns the system to equilibrium slowly relative to changes in voltage the cell experiences via synaptic inputs, which are defined later. As the ion flow is not free, and has some resistance, each ion flow has its own corresponding conductance.

The neuron can emit information in the form of an action potential to communicate with other neurons. A neuron may have an influx of positive ions, typically Na^+, which increases its membrane potential; this process is referred to as depolarization [44]. Hyperpolarization refers to a decrease in the neuron's membrane potential. As a neuron is depolarized, its probability to

generate an action potential increases; the mean membrane potential associated with action potential generation is referred to as the threshold voltage [19]. When a neuron generates an action potential – undergoes a spiking process – its voltage-gated sodium ion channels open first, allowing for an influx of Na^+ [44]. This depolarizes the cell even further, until the sodium channels close and the voltage-gated potassium channels open. When K^+ is released, the system hyperpolarizes to a reset voltage, where the potassium channels are closed. The neuron slowly depolarizes and returns to equilibrium. During this period, referred to as the relative refractory period, the neuron cannot spike. These events are illustrated in Figure 2, which represents the voltage of a neuron as it undergoes action potential generation.

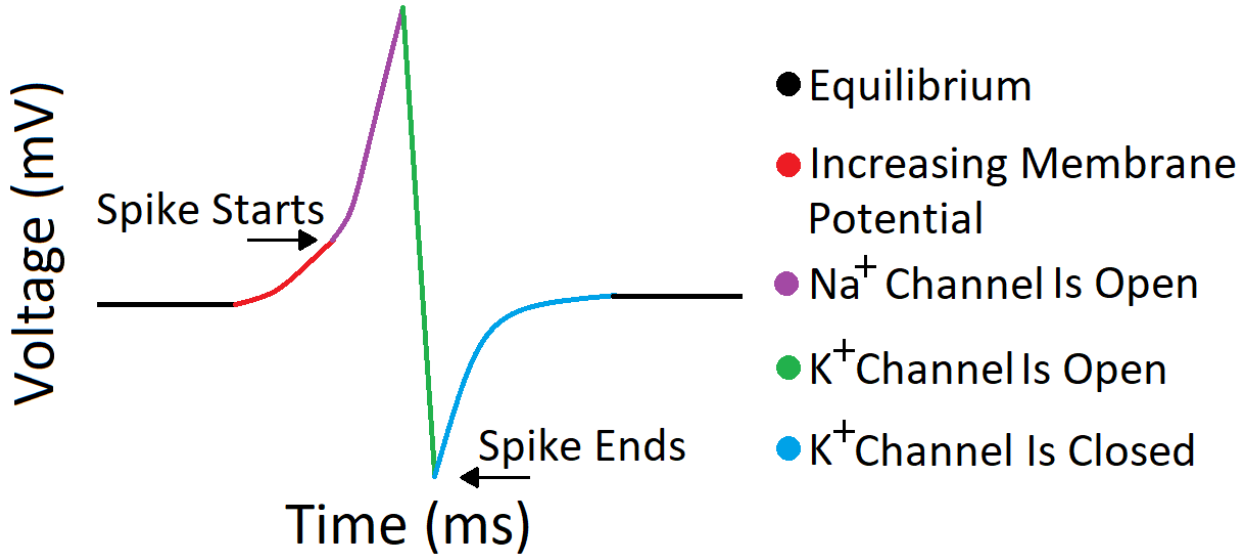

Figure 2: A pictorial representation of a neuron undergoing action potential generation. Increases in the membrane potential, typically from presynaptic inputs, induce a spike event. This spike event opens and closes the Na^+ channels, then opens and closes the K^+ channels, then the system returns to equilibrium.

§1.3: Types of Neurons

While neurons have been shown to be widely diverse, for our work we separate them into two general types: excitatory and inhibitory. Morphological examples of a neuron of each type are given in Figure 1. When a neuron generates an action potential it can either promote the firing of – excite – or prevent the firing of – inhibit – other neurons [1]. The impact of this action potential may depend on many parameters, but for our work it relies solely on the type of the neurons involved (i.e. excitatory or inhibitory).

At the level of an individual synapse, a neuron that relays its action potential is referred to as the presynaptic and the receiving neuron is referred to as the postsynaptic; the overall impact experienced by the postsynaptic neuron is referred to as the synaptic input. The type of the neuron is determined by the neurotransmitter, which is the device the neuron uses to transmit an action potential. Glutamate is the most prevalent excitatory neurotransmitter and uses three different transport systems to send its signal to multiple receptors [19]. Γ-aminobutyric acid (GABA) is the most common inhibitory neurotransmitter and has had its functionality tied to various neurological diseases and disorders, notably epilepsy [19].

§1.4: Modelling Neural Activity: Hodgkin-Huxley

Neurons can be modelled in many different ways, with the two most common conductance-based models in computational neuroscience being the Hodgkin-Huxley model and integrate-and-fire models. Numerous variations of these models exist, which either add or remove features to account for the modeler's needs.

The Hodgkin-Huxley model implements a large degree of biophysical accuracy and was initially based on experimental findings that included the voltage-gated time-dependent sodium and

potassium conductances introduced in §1.2 [7]. The potential difference across the membrane induces an electric field, which was found to cause alterations to the permeability of the membrane. While there are more dynamics involved than just those from sodium and potassium, such as those from chloride ions, the basic Hodgkin-Huxley model coalesces the others into one leakage current. A circuit diagram representative of this model is shown in Figure 3.

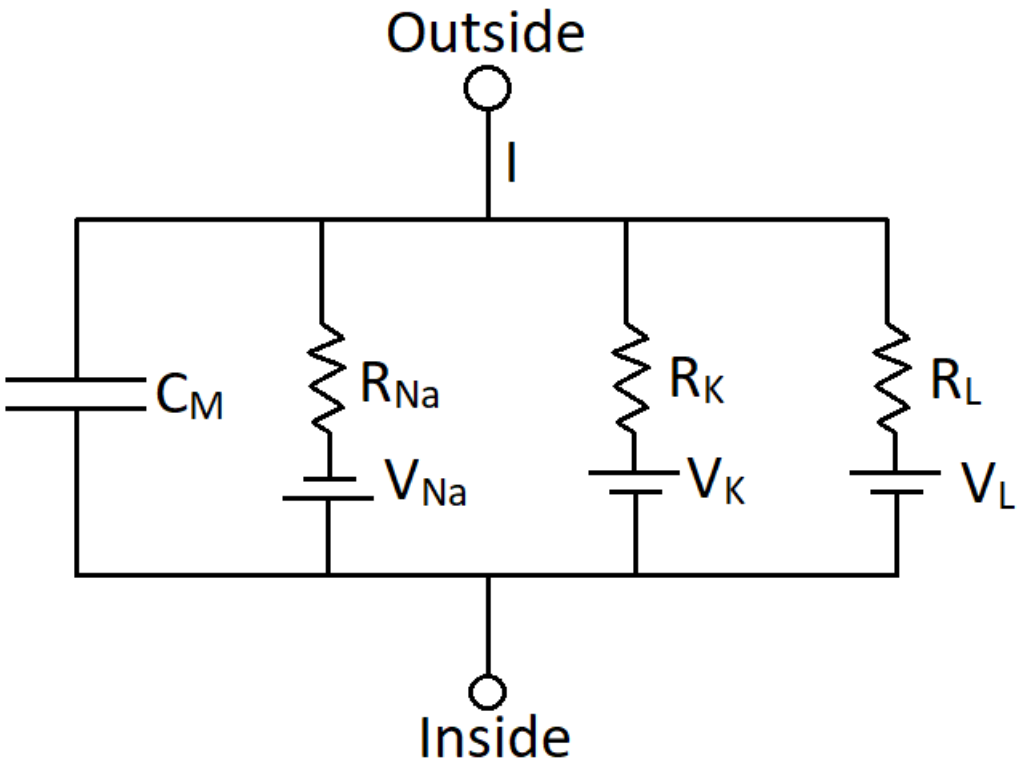

Figure 3: Electrical representation of the Hodgkin-Huxley model. The sodium and potassium channels are accounted for, as well as a third "leakage" current which accounts for the additional impacts from chloride and other ions.

As shown in Figure 3, the overall dynamics of the model are comprised of four separate components: the capacitance of the membrane, the current from sodium flow, the current from potassium flow, and the leakage current. The differential equation for Figure 3 is given by:

$$I = C_M \frac{dV}{dt} + \bar{g}_{Na} m^3 h (V - V_{Na}) + \bar{g}_k n^4 (V - V_K) + \bar{g}_L (V - V_L). \quad (2)$$

For Equation 2, the variables represent the following: the overall current – I –, the voltage – V – , time – t –, the membrane capacitance – C_M – , maximum ionic conductance – $\bar{g}$ –, and the equilibrium potential – V_x – for an index x. The indices relate to each ion accounted for by the model: sodium – Na –, potassium – K –, and all other ions – L –. The variables n, m, and h represent voltage-gated activation and inactivation gates. These gates are voltage-dependent and fluctuate with time. With appropriate parameter selection the model yielded results that agreed very well with experimental values [7].

While the Hodgkin-Huxley model is an incredible tool, it still has its shortcomings. One major disadvantage of the model is that it is sensitive to parameter choice, and a slight change to one of the parameters may completely change the output [8]. The largest disadvantage of the model comes in the form of computational costs. As the equation governing the system is rather complex it takes a long time to solve, which means it would not be suitable for modelling more than a few neurons. Many models either simplify or complicate the Hodgkin-Huxley model proposed here, tailoring it to the modeler's requirements.

§1.5: Modelling Neural Activity: Integrate-and-Fire

Unlike the Hodgkin-Huxley model, integrate-and-fire models of neurons tend to be simplified as much as possible. In doing so, much biophysical accuracy is lost in favor of computational efficiency and low number of parameters. Integrate-and-fire models are based off the idea that the membrane is highly resistive and can act as an insulator, which in a circuit can be represented by a capacitor as it is in the Hodgkin-Huxley model [9]. As current is injected into the neuron the capacitor charges until the point it must discharge, which represents an action potential and occurs

when the voltage is above the designated threshold value. In the integrate-and-fire model, we implement a hard threshold instead of its graded value found in the Hodgkin-Huxley model. After this action potential, the neuron's membrane potential is immediately set to some reset voltage. The membrane is not a perfect insulator as the system will return to equilibrium over time, so using a perfect capacitor alone to model this behaviour is insufficient and a resistive component is needed [17]. Commonly a leakage term is introduced to the system to encapsulate the neuron returning to equilibrium; integrate-and-fire models with this addition are referred to as leaky integrate-and-fire models (LIF). An equation for the basic LIF is given by:

$$\frac{c_m}{g_l}\frac{dV}{dt} = \tau_m \frac{dV}{dt} = E_L - V(t) + R_m I_e(t). \qquad (3)$$

For Equation 3, the variables are as follows: specific membrane capacitance – c_m – , $1/g_l$ the specific membrane resistance – $1/g_l$ – , the voltage – V –, the time – t –, the membrane time constant – τ_m –, the equilibrium voltage – E_L –, the total membrane resistance – R_m –, and the input current – I_e –. The term 'specific' above refers to the variable being per unit area, however in LIF models the neuron is typically represented as a point so morphology is not discussed.

Rather than impacting the solution directly, the membrane time constant changes the rate at which the system grows meaning that in simulations it can be tuned to change the firing rate, introduced in §1.6, without altering the other dynamics. E_L is the membrane voltage that the neuron would return to if there were no input current, which is due to leaking; while the equilibrium voltage is different than the voltage it goes to immediately after an action potential, referred to as the reset voltage, for our work they are treated as the same. Similar to the Hodgkin-Huxley model, a circuit diagram can be created for this basic LIF model and is shown in Figure 4.

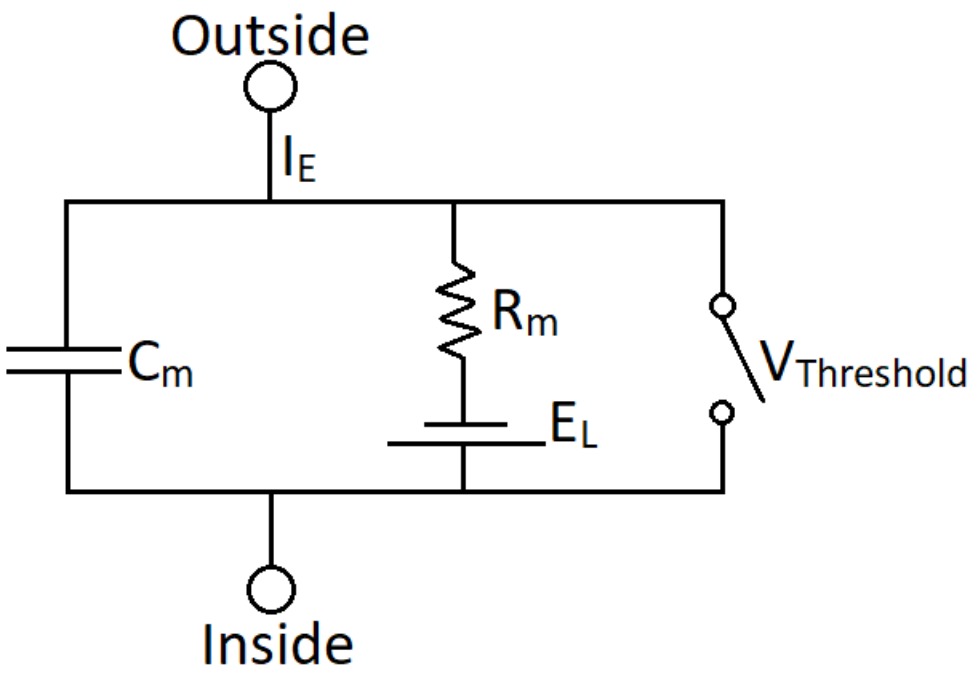

Figure 4: Electrical representation of the leaky integrate-and-fire model. A switch is needed to encapsulate the model's behaviour, although not indicated by Equation 3. When the membrane voltage is larger than the threshold the switch closes, discharging the capacitor.

One large advantage that the LIF model has over the more complex Hodgkin-Huxley model is that it takes substantially less time to numerically solve for the LIF model [7]. This allows the LIF model to simulate a larger number of neurons in substantially less time than more complex models. The simplifications used in LIF models prevent the model from encapsulating biophysical details of a generated action potential, but they can be effective at reproducing the timing of spikes. Computational efficiency and accurate spike timings make LIF models great for investigating the impacts of neuronal communication for populations of neurons.

§1.6: Metrics for Quantifying Neural Activity

While we have introduced some parameters often used while modelling, we have not put forth any of the tools used for analysis. We primarily use the temporal scale to investigate systems with

linear currents while we use the frequency domain to analyze oscillatory networks. The first tool for analysis we put forward is the firing rate – *r* – which is given mathematically by:

$$r = \frac{\#\ of\ Spikes}{Time\ Interval}. \tag{4}$$

Time-averaged firing rates have been shown to range from < 1 Hz to tens of Hertz for the same part of the brain, but for our work we typically stay in the regime of 5-20 Hz. This is because it relates to the most common form of seizure, which is discussed in more detail in §1.7.

When "frequency of firing" is discussed, we are typically referring to this firing rate. There are three different frequencies that are important, and as such attention must be paid to which frequency is being referred to. The firing rate, the exogenous – a.k.a driving – frequency, and the endogenous – a.k.a resonant – frequency are all used when discussing our network.

If two neurons are fully synchronous, they fire at the same time. Extending the term synchronous to a network refers qualitatively to how closely neurons tend to fire in relation to one another [1]. Equations 5-8 introduce a measurement called the synchrony measure – *S* – which aims to quantify synchrony [14]:

$$S = \frac{v}{\frac{1}{N}\sum_{i=1}^{N} v_i} = \frac{Var[< V >]}{< Var[V_i] >} \tag{5}$$

$$v = < V(t)^2 > - < V(t) >^2 = Var[< V >] \tag{6}$$

$$v_i = < V_i(t)^2 > - < V_i(t) >^2 = Var[V_i], \tag{7}$$

where the mean membrane potential is given by

$$V(t) = \frac{1}{N}\sum_{i=1}^{N} V_i(t). \tag{8}$$

A synchrony measure of 1 indicates perfect synchrony and a synchrony measure of 0 indicates asynchronous activity. Rather than using spikes to determine the synchrony measure, voltages and their time averages – indicated by <> – are used. The time averages are used to determine the time variances – v – of the voltages. While the synchrony measure allows for similarities between neurons to be quantified, the measure begins to have shortcomings when heterogeneity is introduced. This is because the synchrony measure uses voltages: even if two heterogenous neurons spike at the same time their thresholds and therefore voltages may be different, resulting in a synchrony measure below 1. Heterogeneity is discussed more in Chapters 2 and 3. Rasterplots, which graphically represent spike timings of a neural population, illustrating high and low synchrony are given in Figure 5. These were generated via the model introduced in Chapter 2.

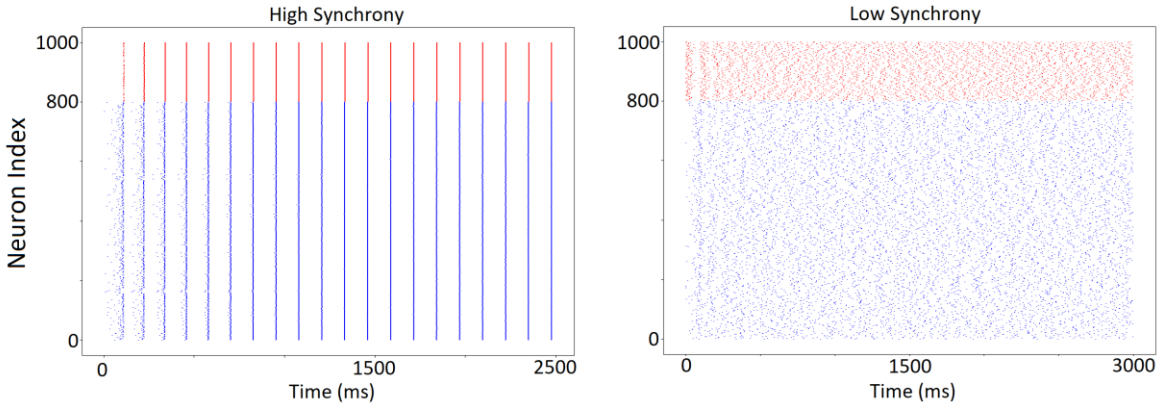

Figure 5: Rasterplots indicating high and low synchrony; in the high synchrony case, left, all neurons fire around the same time, while in the low synchrony – or asynchronous – case, right, action potentials seem to have no correlation between the neurons. Each dot of the rasterplot represents a spike at a given time for its corresponding neuron. Inhibitory neurons are in red while excitatory neurons are in blue.

When oscillations are present in a network, characterizing the system's frequencies inevitably becomes more important. We use a Fourier transform to transition from the temporal to frequency domain to investigate the frequency content of such oscillations. We apply the Fourier transform to the firing rate, take its magnitude, and square the result to yield the spectral power – P –; this process is referred to as spectral analysis [13]. The short form equation for the spectral power is given by:

$$P = |\mathcal{F}(r)|^2, \tag{9}$$

with the full form for the Fourier transform – $\mathcal{F}$ – given in the appendix.

Qualitatively, the spectral power associated with a specific frequency represents the magnitude of the contribution that the frequency has on the network's firing activity. Spectral analysis yields a set of values at discrete frequencies, and therefore values of spectral powers must be investigated relative to others. Spectral analysis is useful as it may indicate behaviour and patterns that are not clearly visible when firing is investigated in the time domain.

§1.7: Synchrony and Epilepsy

Synchrony, or the lack there of, plays a vital role in healthy brain function and neuronal communication. Shifts in synchronization are notably observed in various neurological disorders, such as epilepsy [15]. Epilepsy is characterized by a sudden shift into rhythmic firing and enhanced synchronization, called recurrent seizures. Various hypotheses have been put forward for why seizures might occur, such as decreased inhibition or enhanced excitation for neurons in epileptic tissue [15]. It has also been shown that epileptic tissue, which is intrinsically more prone to seizure, displays lower levels of biophysical heterogeneity compared to healthy controls [16].

Often seizures are initially localized to small neuronal clusters and are referred to as microseizures; projections from these microseizures play a role in propagating signals across neural regions and may cause seizures in nearby regions [15]. Electrical recordings shown in Figure 6A are taken from two different parts of the brain; the second seizes a few seconds after the first, suggesting a propagating signal evoking a seizure downstream. A visual diagram illustrating the propagating signal from a microseizure is shown in 6B.

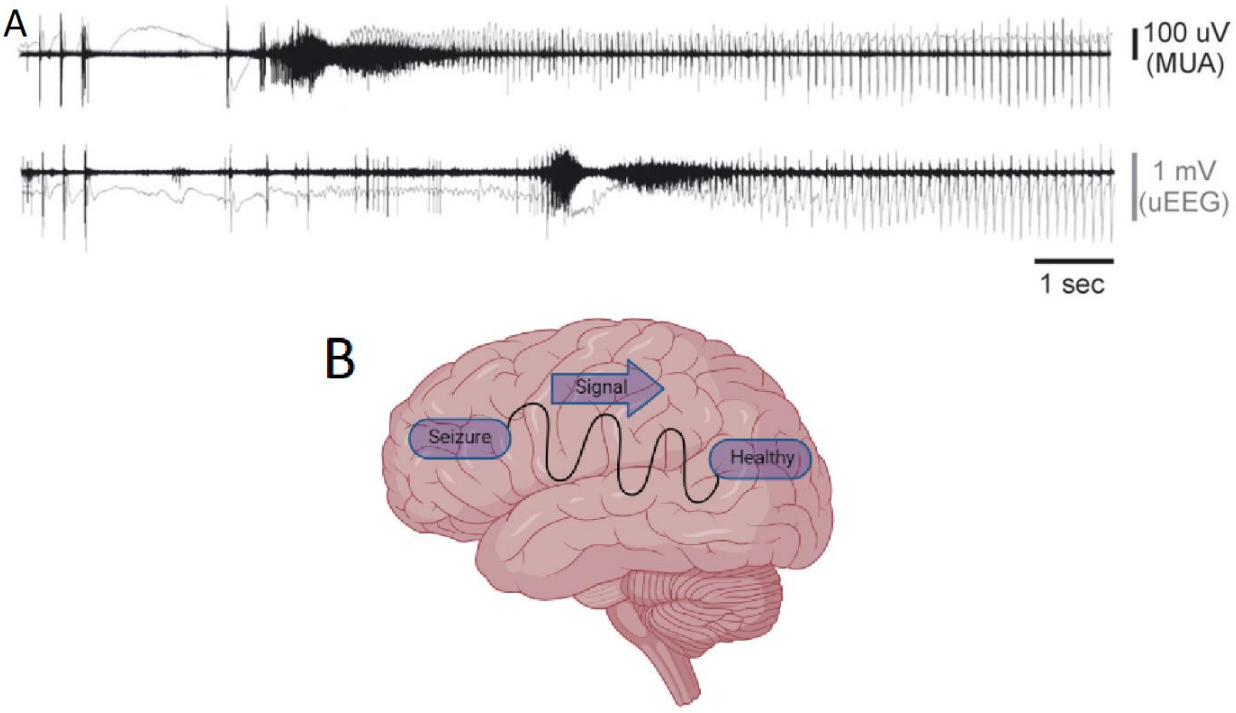

Figure 6: (A) Electrophysiological readings from two parts of the brain, 3 mm apart, taken with permission from [15]. A microseizure in the upper region propagates to the second region, pushing it towards an epileptic state. (B) A pictorial representation of a seizure-like oscillatory signal propagating from one section of the brain to another.

The most common form of seizure, which is prevalent in over 30% of cases, exhibits rhythmic oscillations ranging from 14-97 Hz with a median of 36 Hz [28]. As this range is quite large, we focus on the lower end of the spectrum to narrow our investigation; we also investigate below 14 Hz to view what transitions may occur when entering such a frequency range. It has been shown that frequencies around this region may cause the neurons to become entrained, with firing behaviour being dominated by the imposed oscillatory properties and causing synchronous dynamics [43]. The impact of microseizures on neighboring regions can be modelled, at first order, by an oscillatory periodic input at a given frequency. We refer to this response as seizure-like behaviour. In our work, we maintain a natural firing rate of all neurons between 5 Hz and 20 Hz when no oscillatory component is present to remain near the exogenous frequencies that will ultimately be superimposed on the dynamics of our system.

Chapter 2

Modelling Networks of Neurons

§2.0: Chapter Summary

In chapter 1 we introduced a leaky integrate-and-fire model, and in this chapter we add more detail to the basic model and define the model used in our research. We define mathematically how both neural signals and heterogeneity are represented in our model. We detour from discussing our leaky integrate-and-fire explicitly to explore mean-field approximations. For this we start with an overview of why we use mean-field models and some of their history within the realm of neuroscience, and its application to integrate-and-fire models. We show the resulting equations and attempt to reproduce previously published work. We conclude with a brief discussion on the success of reproducing results and talk about both what it does well and where it suffers as an approach.

§2.1: Leaky Integrate-and-Fire Network Model

We propose a leaky integrate-and-fire network model of inhibitory and excitatory neurons to better understand what roles different variables play in seizure-like behaviour. Previous work has shown that decreased inhibition and enhanced excitation lead to increased synchrony, and that heterogeneity is reduced in epileptic neural tissue [15, 16]. We hypothesize that when a seizure-like input is introduced to an asynchronous network, similar to a region experiencing the impact of a nearby microseizure, that the system may shift to seizure-like behaviour depending on the levels of excitation, inhibition, and heterogeneity. We find results consistent with both previously published work and this hypothesis, as well as additional new behaviour relating to heterogeneity's impact on resonant frequencies.

The equations governing our computational model are given by:

$$\tau_m \frac{dV_i^E}{dt} = E_L - V_i^E(t) + V_{i,Noise}{}^E + R_m I_e^E(t) + s_{IE}(t) + s_{EE}(t) \quad (10)$$

$$\tau_m \frac{dV_i^I}{dt} = E_L - V_i^I(t) + V_{i,Noise}{}^I + R_m I_e^I(t) + s_{II}(t) + s_{EI}(t), \quad (11)$$

where synaptic inputs are given by

$$s_{mn}(t) = \frac{1}{N_m} \sum_{m=1}^{N_m} w_{m,n}\, \delta(F_m(t-1) - 1). \quad (12)$$

The first addition we make to the basic LIF model is a noise term, which biologically would arise from small fluctuations to the input current. Rather than incorporating the noise in the current directly, and hence having it multiplied by the membrane resistance, we implement a voltage term for the noise instead which is represented by V_{Noise} which follows a Gaussian distribution of mean 0 mV with some variance. We also separate the equation outlined in §1.6 into excitatory and inhibitory types, which are indicated by E and I superscripts respectively. The parameters governing synaptic connectivity, $w_{m,n}$ in Equation 12, are summed over the presynaptic neurons' firing events and are explained in detail in §2.2.

§2.2: Synaptic Coupling

We introduce connectivity between cells to our system in the form of static synaptic weights. The term static refers to the fact that the amplitude of a post-synaptic response does not change over the course of a simulation or between different cells of the same type. Synaptic plasticity, which refers to adaptive synaptic weights, is not used for the models put forward in this work [1, 6]. The synaptic weights – $w_{m,n}$ – are comprised of the four signal-reception permutations previously

described in §1.3, and the mathematical equation governing the total signal received by a neuron n for one permutation is given by s in Equation 12.

The network we use, besides that shown in §2.6 and §2.7, is all-to-all connected meaning that all neurons are synaptically coupled with one another. In other words, all connections are realized, and the connection probability between any two neurons is 1. The indicators m and n represent the neuron type for the presynaptic and postsynaptic cells respectively. $F_m(t)$ is equal to 1 if the neuron m spiked at time t, and 0 otherwise. The Dirac delta function is used within the sum to clearly indicate this discontinuous behaviour. The weights are divided by the number of neurons in the presynaptic type to follow the scaling put forward in [22]. A pictorial explanation of the connections is given in Figure 7A, with a matrix representation of what is being summed over for any neuron given in Figure 7B.

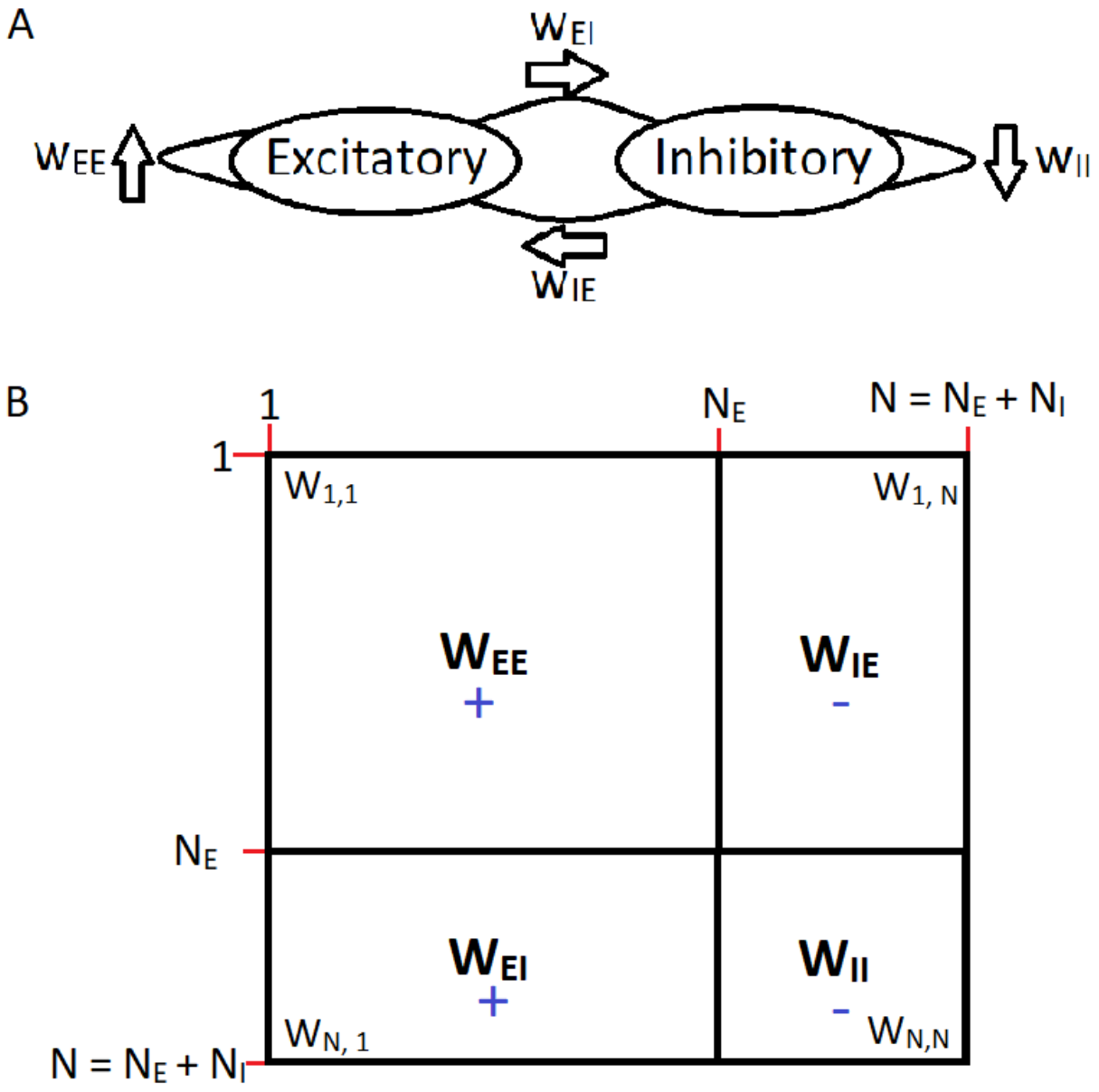

Figure 7: A) A pictorial representation of the connections of weights between excitatory and inhibitory neuron types. B) Matrix representation of the synaptic weights $w_{m,n}$. When a row is multiplied by a firing vector, which has entries of 0 unless a presynaptic neuron fired in which case its corresponding entry is 1, a resulting value is determined which is sent to the postsynaptic neuron. E represents excitatory cells, I represents inhibitory cells, and N represents the total number of neurons. The values for these weights are determined in §3.2.

§2.3: Heterogeneity

High levels of diversity have been shown between types of neurons, and even within the same type of neuron [23]. One impact of heterogeneity that has been shown is its influence on the correlation of spikes in a network, specifically that heterogeneity promotes ungrouped firing [24]. As such, seizures are less likely to occur in systems with high levels of heterogeneity [25]. This also means that the various factors that are associated with a loss of heterogeneity could equivalently be thought of as promoters of seizures and thus epilepsy [16]. Due to its biological relevance in conjunction with our desire to investigate seizures, heterogeneity must be accounted for in our model.

We implement heterogeneity on a cell-specific level by stochastically determining their excitability; we follow the model used by both Mejias & Longtin, and Rich et al. [26, 16]. These models remove the uniform threshold of the neurons and instead implement a statistical one. The threshold values across cells are normally distributed about some mean value with a standard deviation σ. Each cell's threshold is initially sampled from this distribution, and each neuron maintains its threshold value for all times. Thresholds of excitatory and inhibitory neurons may be handled separately, with the standard deviation of excitatory thresholds being given by σ_E and inhibitory thresholds by σ_I; these standard deviations are equivalently called the heterogeneity values, and a pictorial representation of what this means is shown in Figure 8. Biophysical heterogeneity can arise in many ways, such as through membrane resistances or additional biophysical parameters. Variability of thresholds is used because it encapsulates the resultant changes of excitability that arise with neural diversity in a straightforward way.

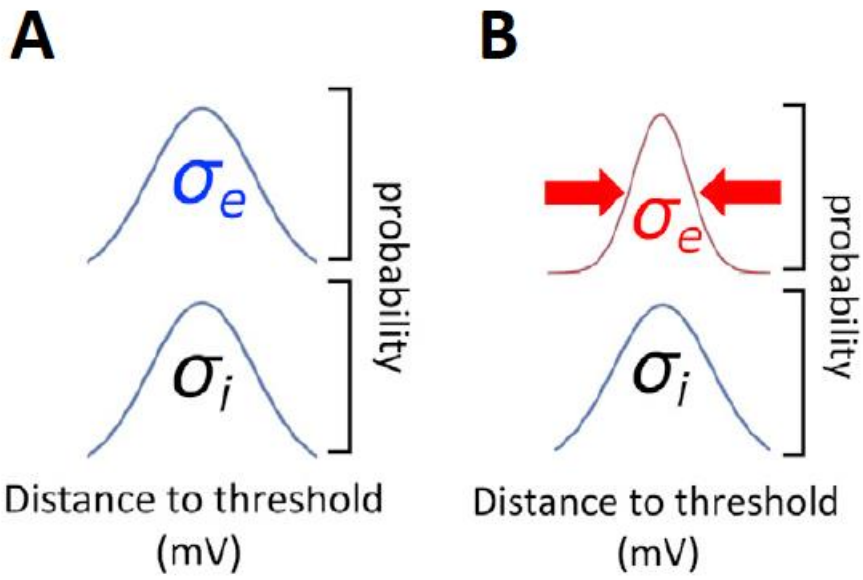

Figure 8: Pictorial representation of the excitability distributions for neurons with different threshold heterogeneities, taken with permission from [16]. The excitatory heterogeneity decreases from (A) to (B), as indicated by the decrease in peak width. The heterogeneity seen in (A) is representative of healthy tissue while that in (B) represents epileptic tissue.

§2.4: History of Mean-field Theories

Due to the intrinsic complexities of neuronal networks, both in experimental systems and theoretical models, an analytical model that simplifies the system to a mean behaviour is beneficial in exploring more general behaviour. Mean-field theories (MFTs) in neuroscience aim to do this, and various representations have been derived with different conditions and features. By developing a mean-field approximation for a specific model, which often does not have an analytical solution, the numerical solutions for the model can be compared to those derived analytically or numerically for the mean-field equivalent.

One of the earliest developments of a MFT was completed by Wilson and Cowan [42]. Using a system of nonlinear equations, they investigated the dynamics of coupled populations containing

both excitatory and inhibitory type neurons. While their work emphasized population properties, 15 years later Leon Cooper developed a MFT based on physiological details. Cooper began by deriving a mathematical theory for the single cell, aiming to create a model that captured the evolution dynamics of synaptic junctions [29]. He then explored how this model would need to change to include network dynamics and other anatomical details [30]. Once this more detailed model was developed, a mean field approximation was proposed that aimed to display the same qualitative behaviour as previously investigated [31]. Future developments have built upon this work, basing MFTs on leaky integrate-and-fire (LIF) models with neural coupling; this work has shown that inhibitory interactions cannot ensure a stable asynchronous state [32, 33]. Variations have been made to model sparsely connected networks, where there is a low probability of neural coupling, and results have been compared to simulated data for LIF networks [34, 26].

§2.5: Our Application of Mean-field Representation

We directly followed the mean-field model put forward by Mejias and Longtin [26]. The mean membrane potentials obey the differential equations

$$\tau_m \frac{dV_i^E}{dt} = \mu_E(t) - V_i(t) + \phi_E(t)\sqrt{\tau_m}\xi_i(t) \tag{13}$$

$$\tau_m \frac{dV_i^I}{dt} = \mu_I(t) - V_i(t) + \phi_I(t)\sqrt{\tau_m}\xi_i(t), \tag{14}$$

where,

$$\mu_E(t) = \mu_0^E + \tau_m K\gamma w_{EE} v_E(t) + \tau_m K(1-\gamma) w_{IE} v_I(t) \tag{15}$$

$$\mu_I(t) = \mu_0^I + \tau_m K\gamma w_{EI} v_E(t) + \tau_m K(1-\gamma) w_{II} v_I(t), \quad (16)$$

represent the main inputs to the cells. The system is driven by noise, meaning that an independent neuron only spikes due to membrane fluctuations caused by noise. The variances of noise are given by

$$|\phi_E(t)|^2 = \phi^2 + \tau_m K\gamma w_{EE}^2 v_E(t) + \tau_m K(1-\gamma) w_{IE}^2 v_I(t) \quad (17)$$

$$|\phi_I(t)|^2 = \phi^2 + \tau_m K\gamma w_{EI}^2 v_E(t) + \tau_m K(1-\gamma) w_{II}^2 v_I(t), \quad (18)$$

where υ_E and υ_I represent the firing rate, with its inverse given by

$$v_{a,i}^{-1} = \tau_{ref} + \tau_m \int_{y_r^{a,i}}^{y_V^{a,i}} G(z)dz. \quad (19)$$

Here a denotes the type of neuron, and

$$y_V^{a,i} = \frac{V_{a,i} - \mu_a}{\sigma_a} \quad (20)$$

$$y_r^{a,i} = \frac{V_r - \mu_a}{\sigma_a} \quad (21)$$

$$G(z) = \sqrt{\pi}\exp(z^2)(1 + \mathrm{erf}(z)). \quad (22)$$

As the variables used in our model differ from those put forward in [26], we begin by finding the mathematical equivalents. For the sake of simplicity, when explaining the variables an a index refers to either an excitatory – E – or inhibitory – I – type of neurons. $\phi_a(t)\sqrt{\tau_m}\xi_i(t)$ takes place

of V_{Noise} in our system, where $\phi_a(t)\sqrt{\tau_m}$ relates to the standard deviation of our noise while $\xi_i(t)$ indicates Gaussian white noise. μ_0^a is equal to $R_m I_e^a(t)$, while the other variables in $\mu_a(t)$ describe the neural coupling in the network. K is the total number of neurons multiplied by the probability of connection, while γ dictates the number of neurons in each type. w_{aa} is the coupling weight, while v_a is the mean firing rate. τ_{ref} is the refractory time, and ϕ is the standard deviation of noise.

An extra contingency was added in numerical simulations. To prevent the case of a neuron having a threshold value too close to, or below, the reset voltage, any neuron that had a threshold generated below one millivolt above the reset voltage was instead attributed a threshold at the mean value. This is unlikely to occur for low heterogeneities, but as heterogeneity increases so does this likelihood. This is because of statistical properties associated the standard deviation, where an increase in the spread increases the probability of lower thresholds being generated.

§2.6: Mean-field Representation Results

We attempt to reproduce the results seen in [26] to ensure a functioning mean-field model; we also compare our simulated network to our mean-field model to verify alignment of simulation and theory. The values obtained via our mean-field model agree qualitatively and quantitatively, within a few Hertz, with those values obtained via simulation and those seen in [26]. The slight discrepancy likely originates from differences in numerical implementation. For example, while [26] may have explicitly determined convergence via stability analysis of the analytical solution, we use a brute force method to determine if the system has converged. Specifically, we checked if the difference in the mean firing rates at two consecutive simulated time steps was below an acceptable tolerance level.

We do see a general trend of agreement between our mean-field model and simulated LIF results, which is shown in Figure 9. When the excitatory heterogeneity - σ_E - is increased, the average firing rate of both excitatory and inhibitory neurons is increased. This aligns with previous work which investigated heterogeneity on an excitatory network and found that a subgroup of neurons with lower-than-average thresholds and higher firing rates naturally developed [41]. While these neurons naturally have a higher firing rate, their repetitive spiking promotes firing of high-threshold neurons. This prevents neurons with high thresholds from not spiking and increases the firing rate of the whole system [26]. Increasing the heterogeneity of the inhibitory population - σ_I - has more complicated dynamics as it increases its average firing rate, but it decreases the excitatory firing rate. Due to neural coupling, the inhibitory subgroup with higher firing rate develops but decreases the level of excitatory firing; while this will in turn prevent further inhibitory firing, the group of low-threshold inhibitory neurons will still spike. This means that the choice of synaptic weights has important consequences on how the system will respond to heterogeneity.

These results indicate that while our mean-field model does not have high enough precision to replace our LIF model, it may be an effective exploratory tool due to its relative computational efficiency. Any large shift in behaviour that directly impacts the firing rate would be reproduced by the MFT, even if the specific results are not precise. The model begins to deteriorate as high levels of heterogeneity are introduced, so it is most effectively used with low levels of heterogeneity.

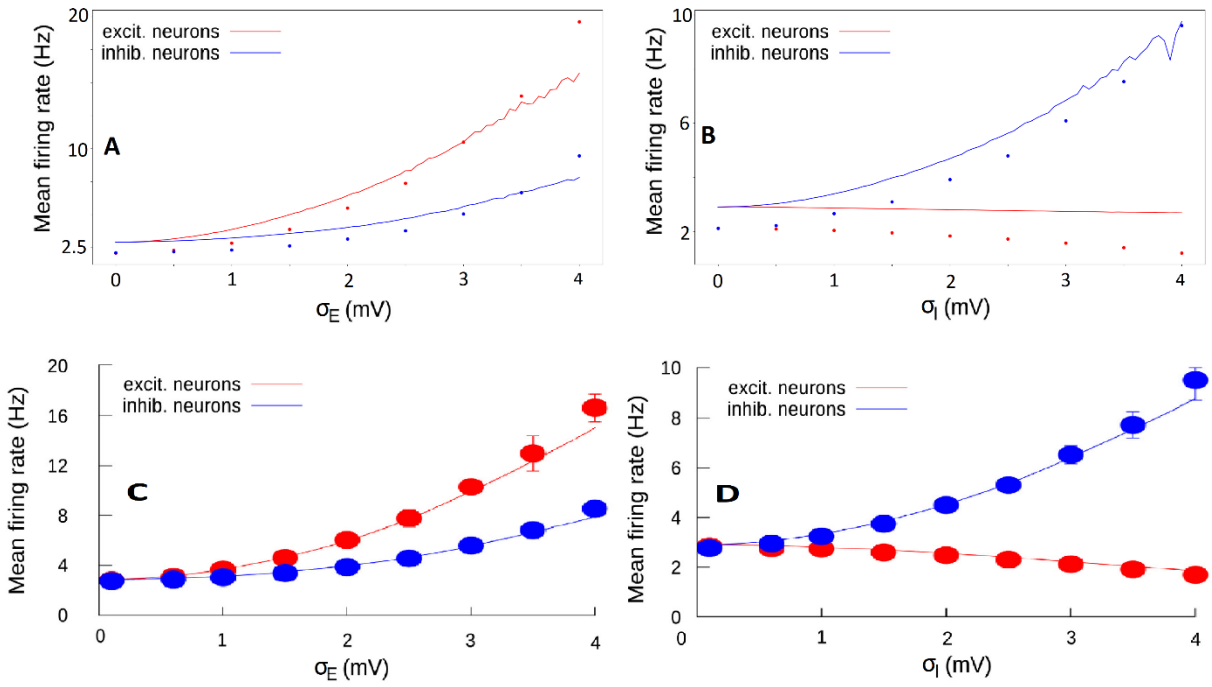

Figure 9: Results comparing the stationary firing rates of the mean field model to simulated results with equal parameters. Simulated LIF results are indicated by the dots while the mean-field results are indicated by the solid lines. A static value of $\sigma_I = 0.1mV$ is used for our work (A) and by Mejias and Longtin (C); a static value of $\sigma_E = 0.1mV$ is used for our work (B) and by Mejias and Longtin (D) [26]. Figure taken with permission from [26].

§2.7: Limitations

Many of the assumptions made in the derivation for the mean-field theory limit its application, such as the network being sparsely connected or all neurons having identical characteristics outside of their synaptic weights. While we have shown that we are able to reproduce the behaviour of the network within a few Hertz of accuracy, we have not pushed this model beyond what has been shown above due to the rest of our work being an all-to-all network with varying degrees of firing correlation including highly correlated spiking. Important assumptions do not hold for our LIF model, such as the fact that we are not always in an asynchronous regime which this mean field

model assumes. The largest difference between the analysis put forward by Mejias and Longtin and those analyzing all-to-all connected networks lies in the stability of synchronization. [26] determines expressions for the parameters that govern stability, and a clear difference in the stability of synchronous and asynchronous systems can be derived. It has been shown that all-to-all networks tend towards synchronous behaviour regardless of initial conditions [35]. This aligns well with our results in §3, where balancing noise and heterogeneity with the synaptic weights is necessary for long-term asynchronous behaviour in systems prone to seizure.

Chapter 3

Response to Seizure-like Stimuli

§3.0: Chapter Summary

While we have previously put forward general models, in this chapter we explain the specifics of our implementation. We begin with the parameters given in [1] for a leaky integrate-and-fire model, and experiment with additional parameters to slowly build a biophysically accurate model of neurons. We start with finding a value of noise that allows for a smooth transition between the subthreshold and suprathreshold firing regimes. Once this is obtained, we implement synaptic weights and begin our search with the values put forward in [22]; due to differences in the models, we quickly find that these values are much too low for our purpose and need to be at least an order of magnitude larger for any effect to be seen. As we want our final system to be prone to seizure, we search for synaptic weights that result in a network with a high variability of synchrony and investigate how heterogeneity impacts the firing of such a region. We add a sinusoidal component to our current to induce oscillatory behaviour and represent a nearby microseizure, and finalize our model by implementing heterogeneity for biophysical accuracy. We conclude this chapter by looking at the results of our model, specifically investigating heterogeneity's role on systems prone to seizure-like behaviour.

§3.1: Preliminary Investigations: Noise

As described in §2.1, the equations governing our network are given by equations 10-13. Before we investigate heterogeneity's impact on a seizure-like system, we must ensure that we are working in a regime that is both realistic and displays the basic properties we desire. We begin with setting the time-independent parameters to those put forward in [1], with specific values outlined in Table 1.

$N_I = 200$	$R_m = 10\ M\Omega$
$N_E = 800$	$E_L = -65\ mV$
$\tau_m = 10\ ms$	$V_{Threshold} = -50\ mV$

Table 1: Standard parameters used throughout this chapter. Changes to these and additional parameters are given as introduced throughout this chapter. N_I is the number of inhibitory neurons, N_E is the number of excitatory neurons, R_m is the membrane resistance, E_L is the reset and equilibrium voltage, $V_{Threshold}$ is the threshold voltage, τ_m is the membrane time constant.

An important feature which results from these parameters is the rheobase, which is defined as "the minimal electric current required to excite a tissue given an indefinitely long time during which the current is applied" [36]. For our work this means the constant value of I_e which is required for a spike to occur when there is no noise in our system, and for the outlined choice of parameters is found to be 1.50 nA. We use the term subthreshold regime to discuss networks with currents below the rheobase where initial spiking occurs due to fluctuations of the noise, and suprathreshold to indicate the regime where the current is above the rheobase. To ensure we have a standard deviation – σ – of noise that is large enough to induce noticeable differences in the solutions between neurons, while not being so large as to completely dominate behaviour, we select a value that produces a smooth curve of the firing rate when transitioning from the subthreshold to the suprathreshold regime; this is found to occur at 2 mV, and this transition is shown in Figure 10. This value of noise was maintained in all other simulations.

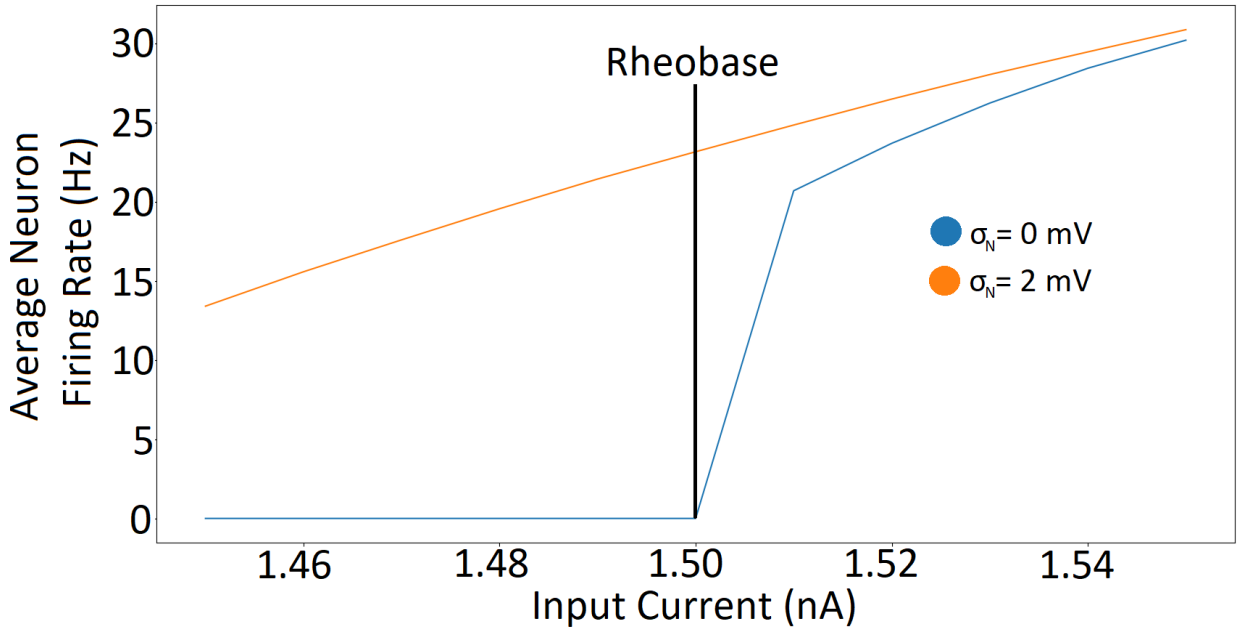

Figure 10: The average firing rate as a function of its input current, also known as the neuron response function. Gaussian distributed noise with mean 0 mV and standard deviation of 2 mV was applied. A smooth transition from the subthreshold regime to that driven by a current above the rheobase value of 1.50 nA is achieved. The case of no noise is shown in blue. A discontinuous spike in firing occurs at the rheobase, indicated by the black line, but due to the resolution of simulation frequencies the first current to drive firing is 1.51 nA.

§3.2: Preliminary Investigations: Spatially Homogenous Synaptic Weights

We implement the synaptic weights as shown by Equation 12 and begin with the values put forward in [22]. These weights are spatially homogenous, meaning that the value of the weight between any two neurons is dictated only by the type of the presynaptic and postsynaptic neurons. As our underlying system has parameters that are quite different than those in [22], we quickly find the synaptic weights are much too small for any dramatic role in our system's dynamics. We instead must explore and look for parameter choices that show some form of E-I interaction; we want to ensure that if every excitatory neuron spikes, such as when driven by a pulse, the response

should have sufficient amplitude to drive most inhibitory neurons to spike. While maintaining the ratio of synaptic weights seen in [22], we determine that we should use weight values that are an order of magnitude larger than those initially tested, due to differences between our model and that in [22]. Rasterplots for different values are shown in Figure 11. We set w_{II} to 0 to reduce our number of dimensions. This assumption is maintained for all our work. We justify this because the value of w_{II} in [22] is an order of magnitude less than all other weights, and I-I coupling accounts for the lowest number of connections in our network.

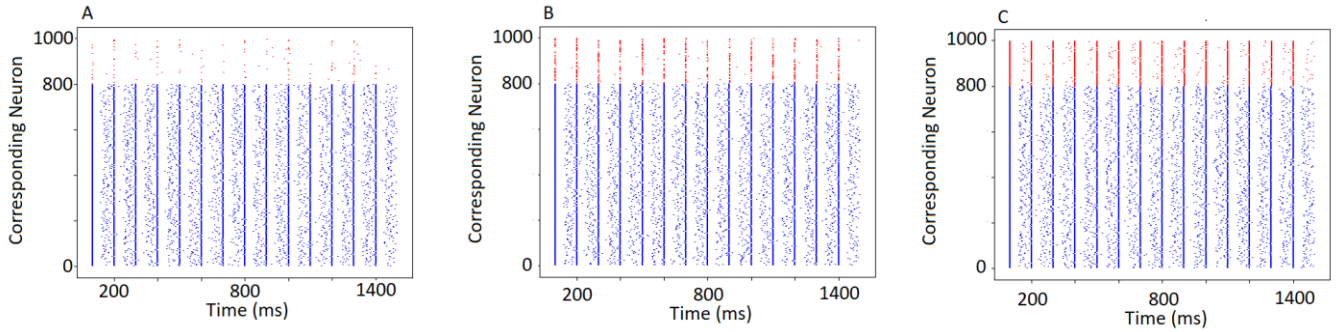

Figure 11: Rasterplots showing excitatory (blue) and inhibitory (red) firing for (A) $w_{EI} = 4$, (B) $w_{EI} = 6$, and (C) $w_{EI} = 20$. A uniform pulse is applied to all excitatory neurons at a rate of 10 Hz to ensure firing, and the inhibitory current is set well below the rheobase of 1.50 nA, at 1.44 nA, so any inhibitory spikes are caused by the excitatory to inhibitory coupling.

Exploration of Figure 11 shows that we need a minimum value of w_{EI} of around 10, as a w_{EI} value of 6 leads to fewer inhibitory spikes than desired at excitatory pulses while $w_{EI} = 20$ shows desired inhibitory spiking behaviour. This figure does not inform us of behavioral shifts that might occur with different synaptic weights as the pulses force some form of synchrony onto our system. We remove the pulses as they were only used to find the minimum w_{EI} required for inhibitory firing and increase τ_m to 30 ms to lower the firing rate so it lies in the desired range of 5-20 Hz. This value of τ_m is used in all simulations moving forward, as is a standard deviation of V_{Noise} of 2 mV.

We perform a three-dimensional scan over w_{IE}, w_{EI}, and w_{EE} to see where shifts in synchrony may occur; this is shown in Figure 12 where the synchrony measure, S, is used. Due to the lack of heterogeneity, the synchrony measure is a good representation of firing synchronicity. When heterogeneity is implemented, and neurons have different threshold voltages, the range of valid voltages for two neurons differ. As such, even if two neurons fire in perfect synchrony their synchrony measure determined by Equation 5 will not be 1. Our work does not investigate another method to determine correlation of spike events.

We find that while w_{EE} plays a major part in determining synchrony, all three synaptic weights play a role. When w_{EI} is increased the system tends towards asynchrony. Increasing the magnitude of w_{IE} seems to indicate a decrease in synchrony, however this is to a lesser extent than changing the other two weights. The increase of synchrony seen with increases of w_{EE} and decreases of w_{EI} confirms the hypotheses discussed in [15] that decreased inhibition and enhanced excitation lead to synchronous firing. As we are interested in the shift from asynchronous to synchronous behaviour, and the reverse, we select a region with high synchrony variability; this occurs mainly in the upper right part of Figure 12 where each red block has a range of synchronies. For this reason, all future simulations use w_{IE} = -30, w_{EI} = 50, and w_{EE} = 10, which is circled in white in Figure 12.

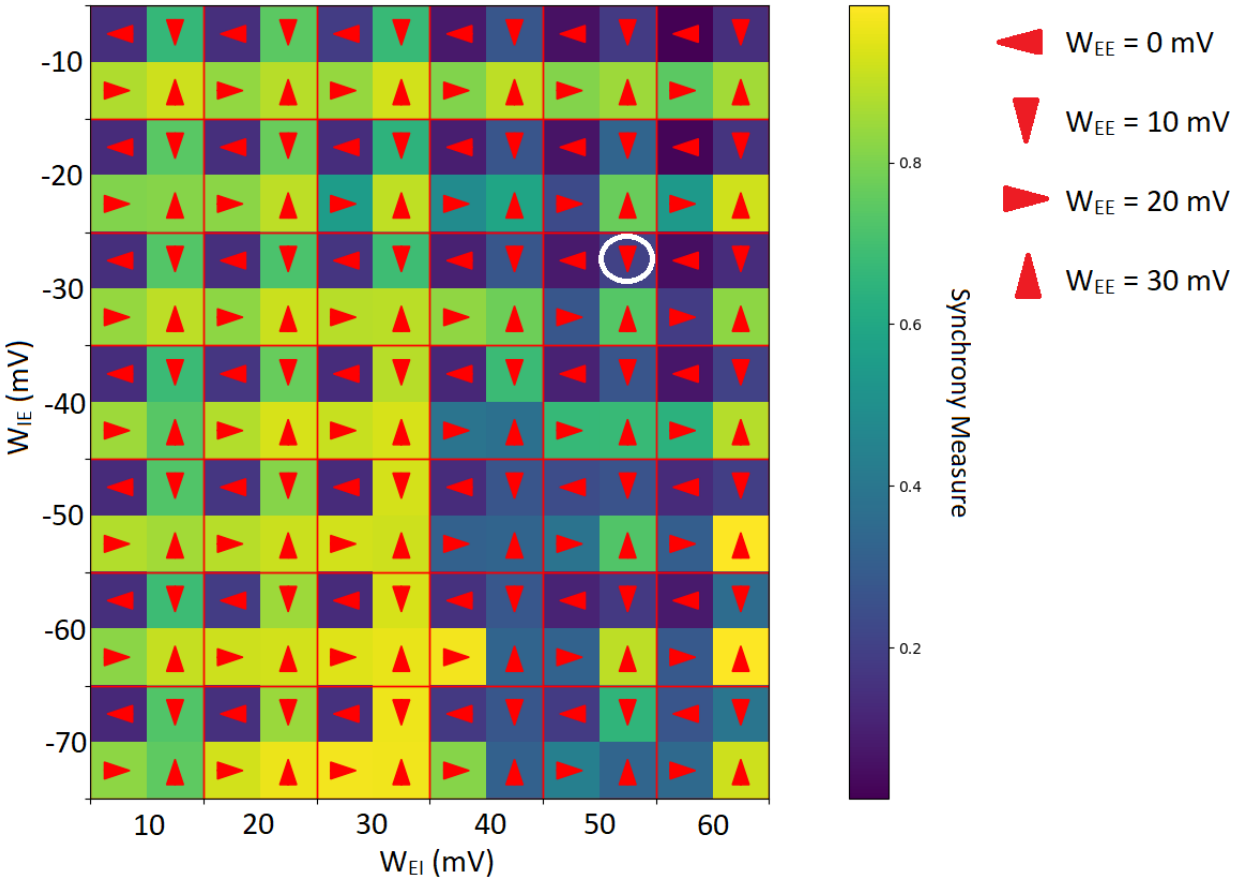

Figure 12: A three-dimensional heatmap investigating how the synchrony measure, *S*, changes with synaptic weights. Sections within a red square share the same values for w_{IE} and w_{EI}. Large shifts in synchrony are seen with the introduction of excitatory-excitatory connections, while the other connections play a role in fine tuning the network's ability to synchronize. The upper right region, with low values of w_{IE}, medium values of w_{EE}, and high values of w_{EI}, is the most prone to shifts in synchrony.

§3.3: Heterogeneity and Firing Rate

We investigate how separating heterogeneity into excitatory and inhibitory components may impact the firing rates of neurons in a LIF model, echoing what was done in the mean-field representation. We set the current – I_e – to 1.51 nA, which is just above the rheobase, for both excitatory and inhibitory neurons (i.e. so we investigate a suprathreshold network). Resulting

asynchronous activity was verified for all simulations. Figure 13 shows that excitatory heterogeneity plays the same role it did in our mean-field model, specifically we see that increasing excitatory heterogeneity increases the average firing rate of both excitatory and inhibitory neurons. Unlike in the mean-field case, inhibitory heterogeneity's effect on the firing rate of excitatory neurons remains unclear. As inhibitory heterogeneity increases the firing rate of inhibitory neurons decreases; this difference in behaviour is likely due to the choice of synaptic weights which is indicated by the complex relation between inhibitory and excitatory heterogeneity shown in Figure 13 B.

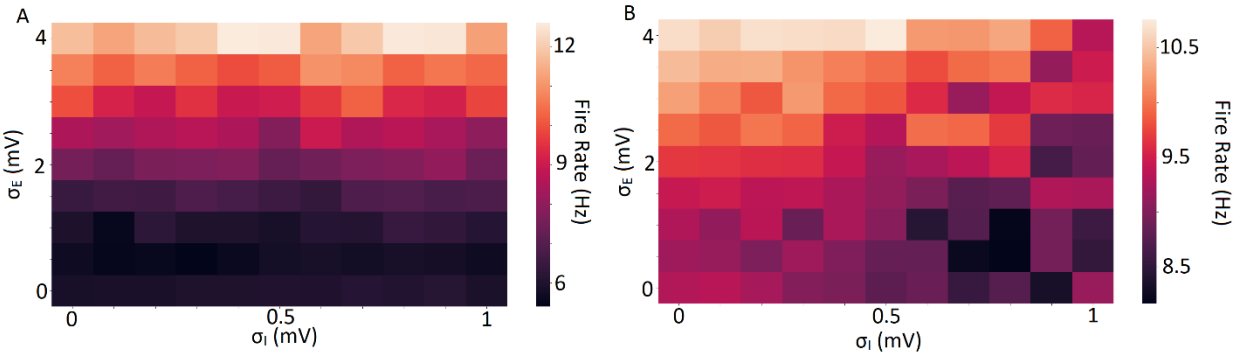

Figure 13: Average firing rates for (A) excitatory and (B) inhibitory neurons scanned over various levels of excitatory and inhibitory heterogeneity. All simulations remain in the asynchronous suprathreshold regime. While increasing the excitatory heterogeneity increases the firing rate of both excitatory and inhibitory neurons, the effect of increasing the inhibitory heterogeneity remains unclear.

§3.4: Periodic Oscillations and Stimuli

We consider seizures to be periodic synchronous spiking, which results in a net periodic pulse of current. As this pulse travels from one region of the brain to another it disperses, losing the sharp peak and becoming more like a sinusoidal wave. A nearby region will undergo the effects of this

wave as well as its normal current. The resulting current experienced by an individual neuron in this region is described as

$$I_e = I_0 + A\sin(2\pi f t). \quad (23)$$

Neural oscillations have been shown to play important roles in both healthy and unhealthy neural systems, and they occur in various frequency bands: delta (<4Hz), theta (4-8Hz), alpha (8-12Hz), beta (12-30Hz), and gamma (>30Hz) [27]. While these natural oscillations are not intrinsically problematic, rhythmic oscillations associated with seizure onset have been shown to occur at frequencies ranging from 1-100Hz [28]. In order to work in a regime that mimics the effect of one of these nearby microseizures, we introduce a time-dependent component to the current to account for nearby oscillatory behaviour and describe this network as seizure-like; this is shown in Equation 23 which splits the overall current into a constant, I_0, component and an oscillatory one with some amplitude, A, and driving frequency, f.

§3.5: Effect of Heterogeneity on Seizure-like Inputs: Time Analysis

Now that we have groundwork for a system that is prone to shifts in synchrony, we superimpose an oscillatory component onto our linear current. We maintain a constant current of 1.51 nA and begin by exploring various driving frequencies and amplitudes of the driving current. As shown in the transition from Figure 14A to 14B, when the oscillation representing a seizure-like input is implemented, the system shifts from asynchrony to synchrony; if the amplitude of the oscillation, A, and the driving frequency, f, are adequate the system becomes synchronous.

We also implement heterogeneity as outlined in chapter 2, but rather than separating it into type specific heterogeneity we apply one value, σ, to represent the diversity of all neurons. Figure 14C shows that with both heterogeneity and oscillatory input, we obtain states with high and low

probability asynchronous firing. These states originate from the oscillatory component, with the high probability of firing correlating to a positive sinusoid and a low probability correlating to a negative sinusoid. This means that heterogeneity sufficiently decorrelates the network, keeping the firing asynchronous and maintaining a healthy neural state, and confirming what is shown in [24].

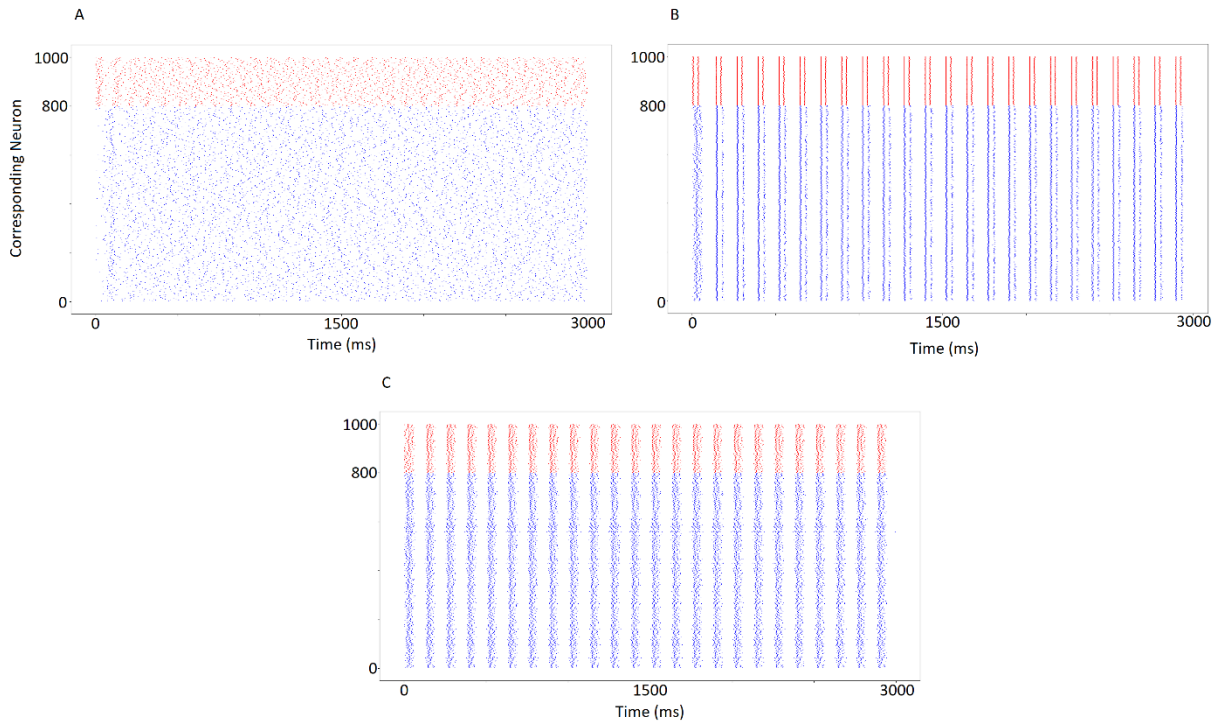

Figure 14: Rasterplots with (A) A = 0 mV, σ = 0 mV, (B) A = 1 mV, σ = 0 mV, and (C) A = 1 mV, σ = 2 mV. We see a transition towards synchrony when the oscillation is incorporated in the system, but away from synchrony when heterogeneity is added.

We also see that increasing the amplitude of the induced oscillatory current makes each state more distinct, separating the firing pattern clearly into high and low probability firing epochs. In the low amplitude cases neurons may fire at any time, while with larger amplitudes the system may prevent spiking during the low probability state. This also makes each state tightly bound to its respective epoch. This is because the magnitude of the slope of the current is larger during the transition

phase between low and high probability of firing for larger amplitudes. Increasing the frequency increases the number of states within a given time frame, as shown in Figure 15. This is expected from general oscillatory properties, but the average firing rate over the entire simulation does not largely change and asynchronous firing is maintained due to heterogeneity decorrelating the network.

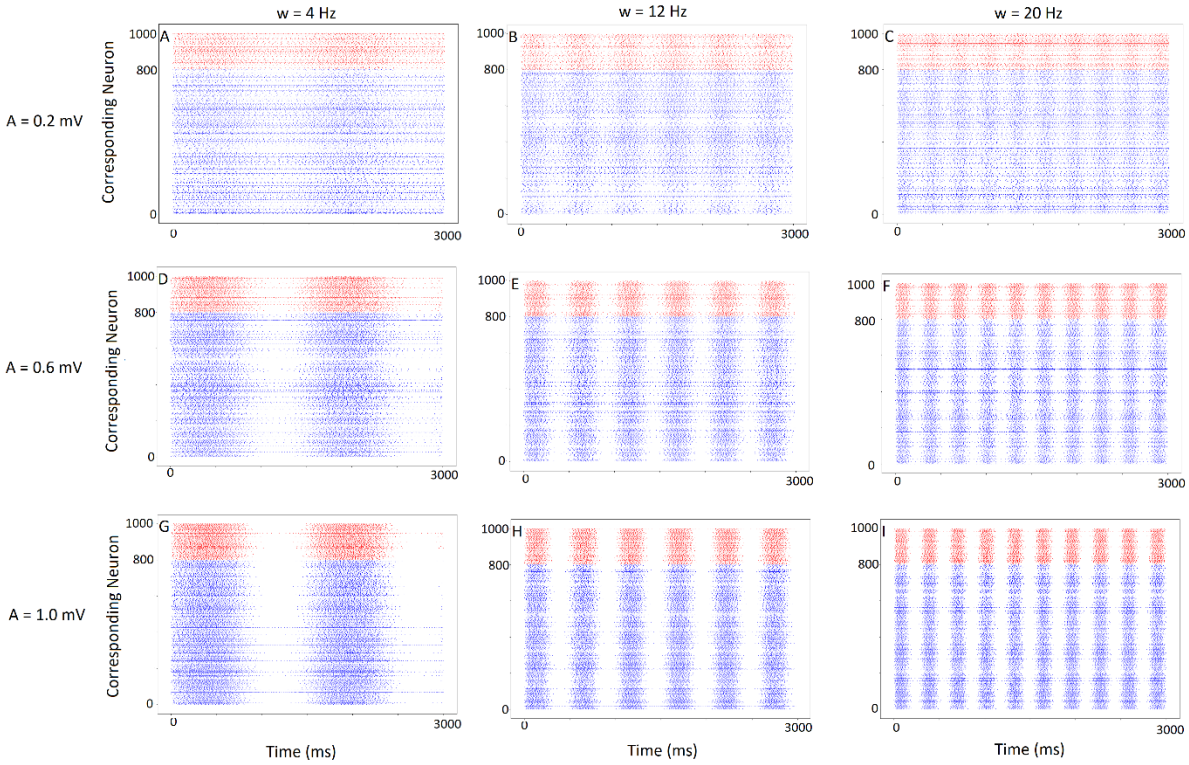

Figure 15: Rasterplots for various input amplitudes and angular frequencies, where $w = 2\pi f$, with $\sigma = 4$ mV. Increasing amplitude decreases the likelihood of spikes in the state with a low firing probability and increases the likelihood of spikes in the state with a high probability of firing. Increasing the angular frequency increases the number of states in a given time period while keeping the average firing rate constant.

While rasterplots are excellent at representing individual data, often an average firing rate is simpler to analyze and is an effective representation of network behaviour. We investigate how the average type specific firing rates change as a function of stimulation frequency, which is shown in Figure 16. We see that while the firing rate of highly heterogeneous systems is independent of the driving frequency, this is not true when there is no heterogeneity. In the latter case the system may become synchronized with the driving frequency, or succinctly entrained. The regions where this occurs are indicated in Figure 16.

This idea of entrainment is consistent with [43] which found that systems with stimulation frequencies similar to ours were shaped by resonance and entrainment. We also see that heterogeneity increases the firing rate of the system when transitioning from σ = 2 mV to σ = 4 mV which is consistent with the concept put forward in [41] that heterogeneity increases the firing rate of a network. While this is true when going from medium to high levels of heterogeneity, it is not seen for low levels. Heterogeneity must first linearize the network before it impacts the firing rate, which is evident in the transition from σ = 0 mV to σ = 2 mV in Figure 16. Interestingly, one type of neuron may be entrained while the other is not since the regions of entrainment are shown to be different. This means that network behaviour plays a role in determining if a system may become entrained. While we are currently unable to comment much on resonance, besides the idea that the resonance frequencies likely lie within the regions of entrainment, this subject is further investigated in §3.6.

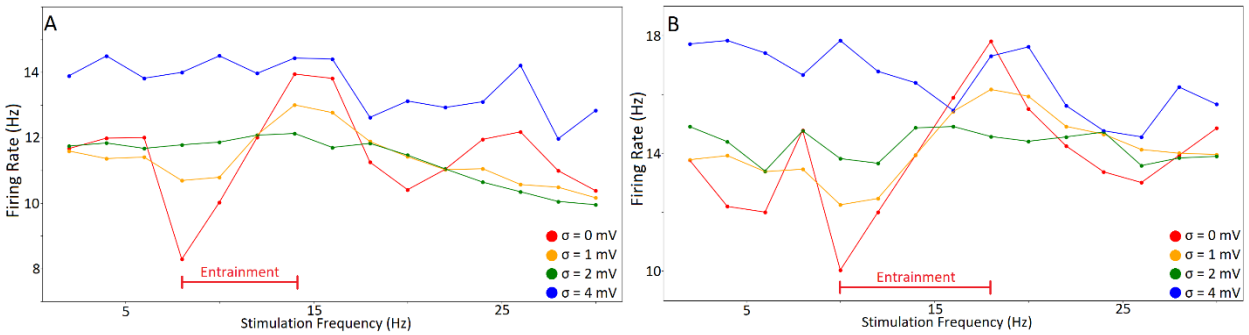

Figure 16: Plots for (A) excitatory and (B) inhibitory firing rates for A = 0.8 mV with various driving frequencies across multiple values of heterogeneity. With no heterogeneity we see peaks in the firing rate of the excitatory type around 14 Hz with a driving frequency of 14 Hz, while inhibitory neurons reach a peak around 18 Hz with a stimulation frequency of 18 Hz. We see in the case of no heterogeneity that neurons may become entrained, while this is not the case for moderately heterogeneous systems. This indicates that heterogeneity decorrelates the system.

§3.6: Effect of Heterogeneity on Seizure-like Inputs: Spectral Analysis

While temporal dynamics have been an effective tool so far, we use spectral analysis to investigate what signals compose our system's solution. We begin by exploring how the stimulation frequency and heterogeneity change the behaviour or values of the spectral power. This is shown in Figure 17 which looks at the spectral power of excitatory neurons with driving frequencies in the delta, theta, and alpha regimes. We expect the spectral power to have a maximum peak at the stimulation frequency with subsequent peaks having lower spectral powers and occurring at integer multiples of the driving frequency, which we refer to as harmonics. While we see this behaviour for a stimulation frequency of 10 Hz regardless of the heterogeneity, the other frequencies are not consistent with our expectations for low levels of heterogeneity. We see that systems with low levels of heterogeneity are most impacted by the endogenous frequency, this is clearest with no heterogeneity and low driving frequencies. This is shown by the fact that higher-order harmonics

do not continue decaying near the resonant frequency that occurs around 28 Hz in Figure 17. As we introduce heterogeneity we see a suppression of resonant frequencies, which is best shown by the plot E. If low levels of heterogeneity were to fully remove the resonant frequencies the graphs would follow our prediction, where harmonic strength decays monotonically; while this is the case with high levels of heterogeneity, it is due to the large suppression of resonant frequencies leading to this behaviour.

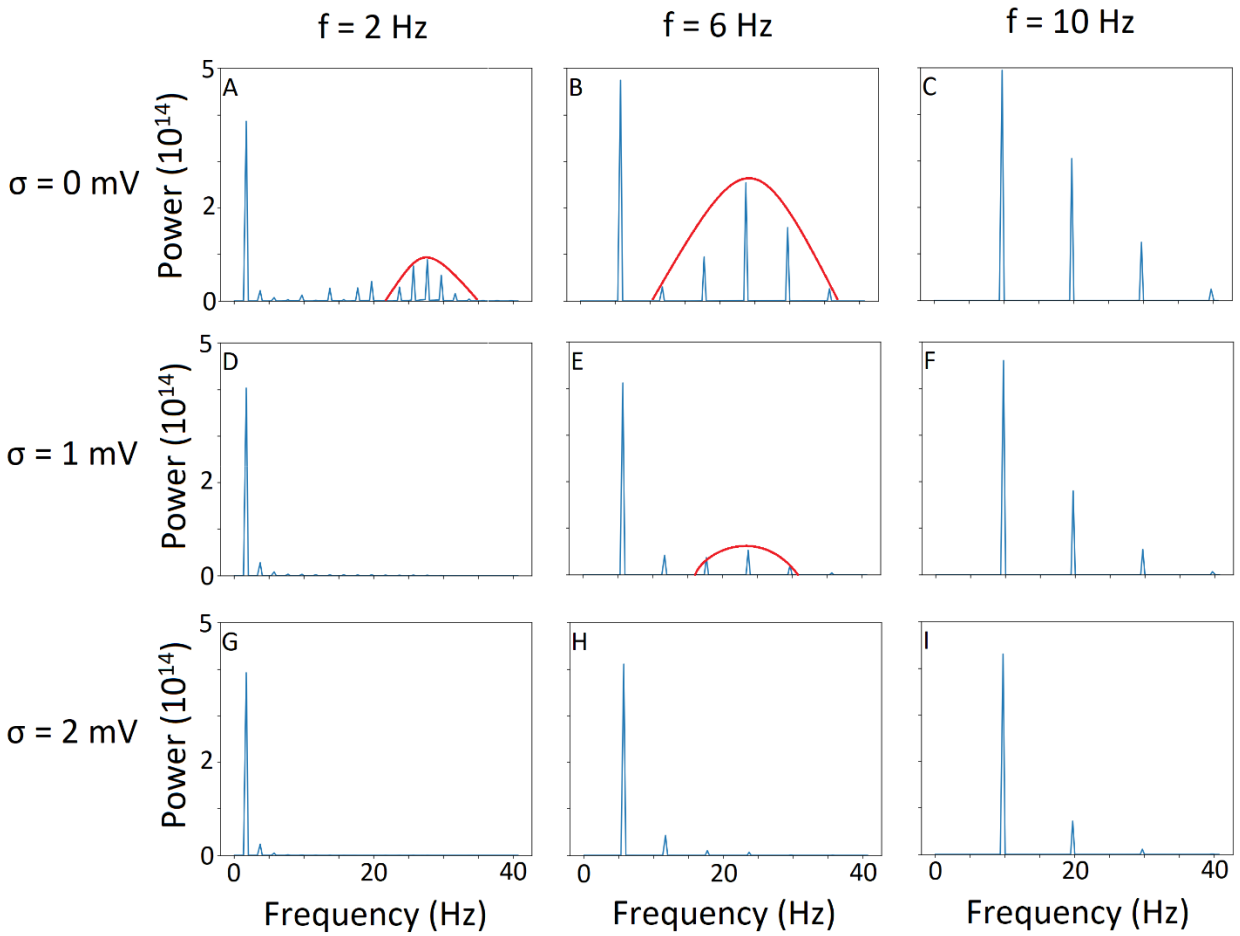

Figure 17: Power spectra for various stimulation frequencies and heterogeneities. No resonance can be seen for plots at 10 Hz. Resonance is indicated in red around 28 Hz, and is seen in A, B, and E. Increasing heterogeneity decreases resonance.

As Figure 17 does not have the resolution to thoroughly investigate lower values of power, we are curious if heterogeneity can change the resonant frequencies in our system. To ensure that heterogeneity truly suppresses the resonant frequencies rather than shift them, we must look at the behaviour across a wide range of frequencies for different values of heterogeneities; this is what the heatmaps in Figure 18 illustrate. Due to resonance, we expect the largest spectral power to occur with a driving frequency matching the endogenous; for excitatory neurons this occurs around 14 Hz in Figure 18. While this is below the frequency we would expect from Figure 17, which shows that resonance occurs around 28 Hz, there may be a few reasons for this. One reason for this may be that when the stimulation frequency is increased the overall maximum spectral power decreases, and this dominates the effect of resonance; we see this decrease in total maximum powers for all heterogeneities. A true resonance peak of 28 Hz would also explain why we see a peak in maximum spectral power at 14 Hz as it would be a subharmonic of the resonant frequency; while 14 Hz has been explained as the maximum entrained frequency of excitatory neurons, from our work it is unclear whether the subharmonic aligning with the entrainment is coincidental or correlated.

If the highest spectral power shifts as heterogeneity is increased, it would indicate that the resonant frequencies change with heterogeneity. If heterogeneity is increased and instead the highest spectral power decreased to be closer to the rest of the powers, it would mean that the resonance is suppressed with heterogeneity, and we see this to be the case.

Figure 19 shows the same behaviour as Figure 18, but for inhibitory neurons. While the qualitative behaviour is the same between inhibitory and excitatory neurons, the quantitative features are different; specifically, the maximum spectral powers are an order of magnitude less for inhibitory neurons, and the resonance frequency is at 18 Hz. Similar to the excitatory neurons, the maximum

entrainment frequency for inhibitory neurons occurs at this peak in our network. While no resonance stands out for inhibitory neurons with a driving frequency of 14 Hz, the average firing rate of inhibitory neurons is 14 Hz when heterogeneity is not included. This means that while a spike in the average firing rate of a neuron type is likely indicative of resonance and entrainment, the relation between endogenous frequencies and the networks firing rate may be coincidental.

Another feature seen for both excitatory and inhibitory neurons is that increasing heterogeneity decreases the spectral powers for higher-order harmonics. The spectral power of the second harmonic, underlined in blue in Figures 18 and 19, decreases as heterogeneity is increased. The logs of the spectral powers are looked at to decrease the contrast, revealing that both higher-order harmonics and subharmonics have not completely vanished and still have some effect on the system. This also indicates that heterogeneity suppresses the response to periodic inputs, leading to the decorrelation of neurons and promoting asynchronous firing in a system experiencing seizure-like inputs.

Since the parameter choices for both inhibitory and excitatory neurons are the same, the difference in resonance and entrainment frequencies must stem from the network dynamics. One difference between excitatory and inhibitory neurons is that, with no heterogeneity and a driving frequency of 2 Hz, there is a missing higher-order harmonic for inhibitory neurons, specifically 8Hz which is indicated by the blue arrow in Figure 19. Since this is only the 4^{th} order harmonic, and can be seen in the heterogenous cases, it means that there is some interference preventing an increase of inhibitory firing for this stimulation frequency. This may stem from excitatory neurons being entrained at 8 Hz while inhibitory neurons are not, as shown in Figure 16.

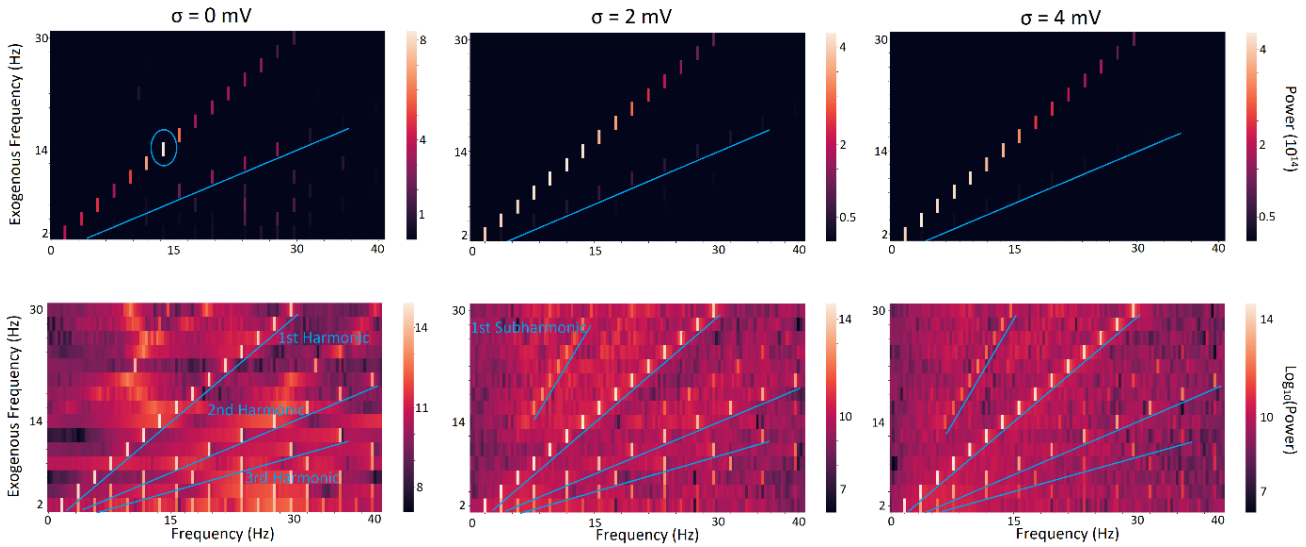

Figure 18: Heatmaps comparing the power spectra for different driving frequencies, with different levels of heterogeneity. These are representative of the excitatory cells. We see that increasing heterogeneity suppresses the endogenous frequency, as well as decreases the power of higher-order harmonics. The upper and lower graphs represent equivalent data, with the logarithmic graphs being used to increase contrast for clearer analysis of behaviour at lower values of power.

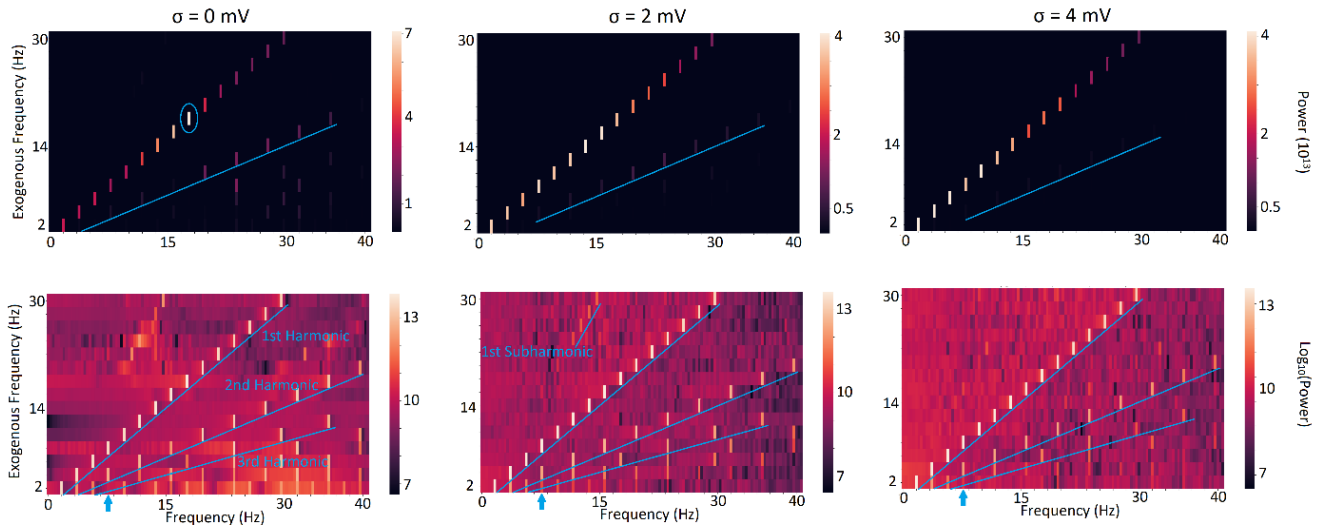

Figure 19: Heatmaps comparing the power spectra for different driving frequencies, with different levels of heterogeneity. These are representative of the inhibitory cells. We see that increasing heterogeneity suppresses the endogenous frequency, as well as decreases the power of higher-order harmonics. With σ = 0 mV we see that a stimulation frequency of 2 Hz does not produce an increase in power at its fourth harmonic at 8 Hz, which is indicated by the blue arrow. The upper and lower graphs represent equivalent data, with the logarithmic graphs being used to increase contrast for clearer analysis of behaviour at lower values of power.

The graphs in Figures 18 and 19 appear highly discretized, however this is due to the low sampling of driving frequencies in our simulations. If more frequencies were sampled, we would expect a clear line along the diagonals for harmonic frequencies, which is indicated by the blue lines in the logarithmic graphs. As the peaks are of interest, we look at how the global maximum powers of a stimulation frequency, which was consistently given by its first-order harmonic, vary with heterogeneity; graphs showing these for both excitatory and inhibitory neurons can be found in Figure 20. We see the same behaviour shown in Figure 18 where increasing heterogeneity suppresses the resonant frequencies while having little impact on the spectral powers far away

from the endogenous frequency. We also see slightly different behaviour in the spectral powers around the resonant frequencies for excitatory and inhibitory neurons. While the maximum spectral powers of excitatory neurons have nearly symmetrical values around their endogenous frequency, inhibitory neurons seem to be skewed such that the frequencies below the resonant value have a greater contribution to the final signal. If this were due to the graphical resolution and the true resonance were to occur at a value such as 17.3 Hz, then the spectral power at 14 Hz would be less than that at 20 Hz. Since this is not the case, and the spectral power at 14 Hz is larger than that at 20 Hz, the lack of symmetry is a feature of the system rather than any graphical effect. Once again, since the parameters are identical for excitatory and inhibitory cells this difference stems from network dynamics.

One interesting feature can be seen for excitatory neurons, and to a less dramatic extent for inhibitory neurons, which again happens at 8 Hz. While the general trend is that increasing heterogeneity either decreases the maximum power or has little impact, 8 Hz seems to increase its maximum power as heterogeneity increases. This, along with the missing harmonic for inhibitory neurons previously pointed out, enforces the idea that certain frequencies behave differently than expected. In terms of a system undergoing seizure-like input from a nearby microseizure, it may indicate that certain frequencies are more likely to promote seizures than others.

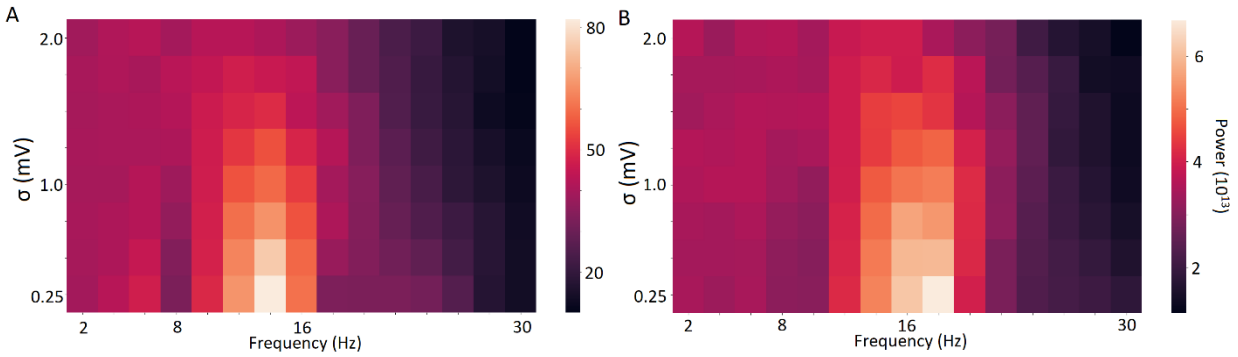

Figure 20: Heatmaps comparing the maximum power at its corresponding driving frequency for (A) excitatory and (B) inhibitory cells at different levels of heterogeneity. The endogenous frequency is shown to be different for each cell type, while the general behaviour is similar.

§3.7: Impact of Type Specific Heterogeneity on Periodic Seizure-like Inputs

Up to this point, we have discussed heterogeneity as one variable for our periodic system, and have not separated it into excitatory and inhibitory neuron types. Biologically, levels of diversity vary from cell to cell, but inhibitory neurons have been shown to have particularly diverse properties [4, 5]. As such it is important to determine if heterogeneity of excitatory, inhibitory, or both types of neurons are predominantly involved in generating our results. We separate heterogeneity into the two neuron types and investigate how their spectral distribution changes with type specific heterogeneity at 8 Hz and 14 Hz; these are show in Figure 21 and Figure 22 for excitatory and inhibitory neurons respectively. We see that it is primarily the corresponding heterogeneity that impacts the power of a neuron with a given type. Maximum spectral powers for excitatory cells primarily change with excitatory heterogeneity, while maximum spectral powers for inhibitory cells primarily vary with inhibitory heterogeneity.

As excitatory heterogeneity is increased, the maximum power tends to decrease; this is shown in Figure 21B. The oddity around a driving frequency of 8 Hz is confirmed in Figure 21A, where

increases in excitatory heterogeneity correlate with an increase in the maximum power. Inhibitory cells, both those at 8 Hz and 14 Hz, decrease their maximum power when the inhibitory heterogeneity is increased. Unlike the excitatory cells, the inhibitory cells do change their maximum power when excitatory heterogeneity is altered. While this seems to have very minor to no impact for a stimulation frequency of 14 Hz, there are clear indicators that show the correlation for 8 Hz. When excitatory heterogeneity is increased, the maximum inhibitory power is increased. This means that an increase in general heterogeneity, as previously investigated, has conflicting components for the maximum power of inhibitory cells.

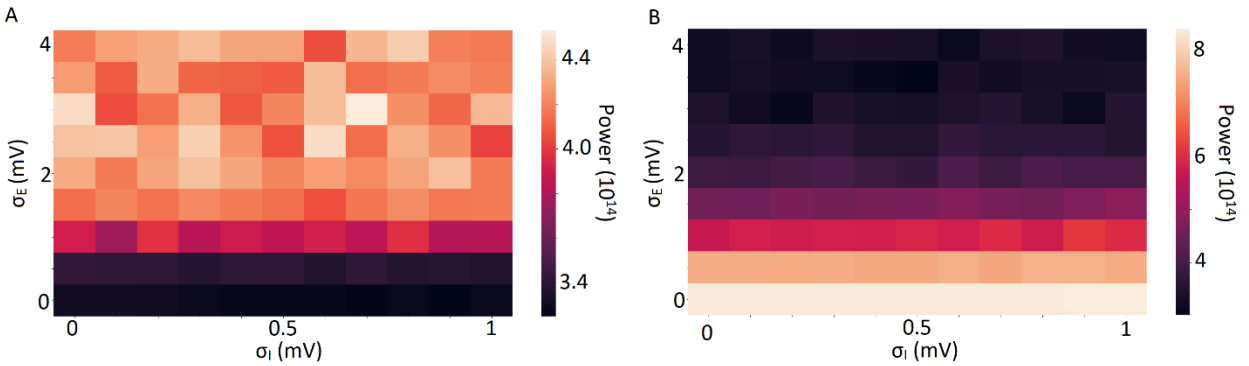

Figure 21: Heatmaps investigating how the maximum power changes with excitatory and inhibitory heterogeneity separately for excitatory neurons at 8 Hz (A) and 14 Hz (B). While inhibitory heterogeneity has no effect, increasing excitatory heterogeneity increases the maximum power at 8 Hz while it decreases the maximum power at 14 Hz.

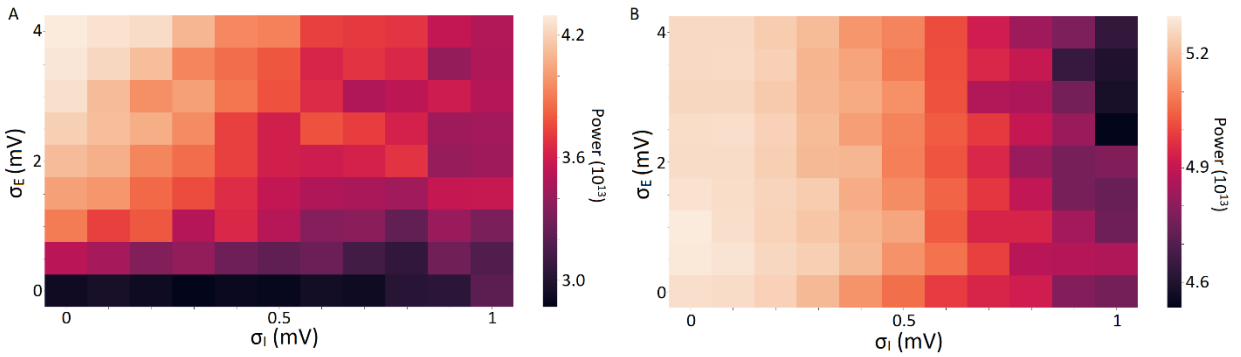

Figure 22: Heatmaps investigating how the maximum power changes with excitatory and inhibitory heterogeneity separately for excitatory neurons at (A) 8 Hz and (B) 14 Hz. Increasing inhibitory heterogeneity increases the maximum power at both 8 Hz and 14 Hz. While increasing excitatory heterogeneity has no impact at 14 Hz, increases in σ_E correlate to increases in maximum inhibitory powers at 8 Hz.

8 Hz has been isolated as an example due to its seemingly unique behaviour, but there are a few reasons this might occur. One reason may be that as heterogeneity is increased the system linearizes. This behaviour has been shown in Figure 16 and would mean that some of the interharmonics – frequencies that are not harmonics or subharmonics – will increase in spectral power while the harmonic peaks decrease. Another factor leading to the oddity at 8 Hz may be that it is the first frequency to produce neural entrainment, and one of the few driving frequencies which increases its average firing rate as heterogeneity is increased from low to medium values. Our data does not have the resolution required to test these hypotheses, but if the simulated data were to have smaller steps between driving frequencies each idea could be tested.

Chapter 4

Final Reflections

§4.0: Chapter Summary

In the previous sections we discussed and put forward a leaky integrate-and-fire (LIF) model to investigate the role that heterogeneity plays on systems that are prone to seizure-like behaviour. We see behaviour that is both consistent with previously documented results, as well as features that are indicative of new properties. In this section we reflect on the reconfirmed observation that introducing heterogeneity decorrelates activity and this new behaviour of heterogeneity suppressing resonance; we also discuss what implications it may have for both models and biophysical systems. We follow this with a discussion of what needs to be done to better understand what defines a resonant frequency; we also put forward some additional biophysical parameters that could be implemented in our model and discuss their impact for a different LIF model. We conclude with some final thoughts on the ideas put forward in this thesis as well as a brief reflection on the thesis and research project as a whole.

§4.1: Scientific Implications

We confirm the idea that heterogeneity decorrelates the system and promotes asynchronous behaviour, mirroring what has been shown biophysically. Specifically, heterogeneity is reduced in systems prone to seizures, and systems with low excitatory heterogeneity are more likely to see changes in synchrony [16]. This confirmation indicates that our model has the parameters required to simulate a functioning network that is representative of epileptogenic regimes. We also confirm that nearby microseizures can induce seizure in an otherwise asynchronous system, and that these oscillations provide a valid candidate mechanism for seizure onset.

From our results we see that introducing heterogeneity suppresses endogenous frequencies in all frequency ranges. When resonance occurs, it may shift the system towards synchronization due to

the entrainment of neuronal firing. Rasterplots are given in Figure 14 that show this effect, and that heterogeneity sufficiently decorrelates this system ensuring asynchronous firing. We also see that heterogeneity suppresses the overall response to seizure-like inputs, with large levels of suppression for higher-order harmonics. While this is the general trend, certain frequencies behave differently; in our simulations 8 Hz is an example of an outlier frequency. The overall takeaway from our simulations is that heterogeneity decorrelates excitatory-inhibitory networks, which is evident both from the output spiking activity and the spectral powers, but certain frequencies may respond differently to increases in heterogeneity.

Understanding the interaction between heterogeneity and resonant frequencies may be vital to determine where shifts in synchrony are more likely to occur. Resonant frequencies play a part in the network dynamics, which is evident when looking at the power spectral density distributions. This means that while the network's behaviour may not be clearly different, certain parameters controlling the system may have an unseen role. Models should use heterogeneity in addition to noise as they impact the background behaviour in different ways. Even [11], which investigates how a wide range of additional parameters impact a leaky integrate-and-fire model's ability to reproduce biophysically accurate spiking, does not account for any form of biological heterogeneity. Previous work, which investigates how the resonance frequencies in a leaky integrate-and-fire network change for various degrees of noise, has failed to account for neural heterogeneity [6].

There are regions of interest within neuroscience where resonant frequencies play an important role in obtaining proper functionality, so balancing the heterogeneity to obtain asynchronous firing while keeping some degree of resonance is important. One example of a region like this is the auditory cortex, where individual differences in neural resonant frequencies are important for gap

detection and speech processing [38]. Work has been done to investigate how the auditory cortex, and other sensory regions that are known to have prevalent resonances, relate the resonance frequency to the region's anatomical volume; even in such a highly biophysical model, heterogeneity and its impact are not accounted for [39]. The auditory region primarily functions in the gamma range of oscillations, while the resonance in our system occurs at lower frequencies [38].

§4.2: Future work

If we were to investigate the auditory system, or any system where we would be interested in the details of the endogenous frequencies, the first step would be to look at what sets the location of the resonant peaks. We show that in networks with identical parameters that resonance occurs at different frequencies for inhibitory and excitatory neurons, meaning that neural coupling plays a role in determining the endogenous frequencies. While it is understandable that the network connectivity has an impact on the difference in peak frequencies, determining the parameters that dictate the general location of the endogenous frequency is required before we are able to investigate regions where resonance is of interest. We use a simple LIF model so additional biophysical features may be needed to properly investigate regimes where resonance is important, such as accounting for spatiotemporal differences that might occur and cause differences in spikes. In the case of the auditory system this would be caused by the interaural time difference, which is the small difference in time that a sound arrives at each ear [40].

While our system is shown to be sufficient in reproducing seizure-like behaviour, additional biophysical parameters could be added to our model for biophysical accuracy. One example of this would be a refractory time, where a neuron cannot fire for some time after it has spiked [11]. This would also solve the problem of a neuron firing at every time step. To avoid this in our network

we impose a hard limit that no threshold voltage can be within 1 mV of the reset voltage. This is sufficient for low levels heterogeneity, but it is likely to cause problems as heterogeneity is increased due to statistical properties of distributions. Refractory times are commonly implemented in models by adding an exponential time component to the threshold, allowing the threshold to decay to a set value as the time since the individual neuron's last spike increases. In conjunction with neural coupling, or more generally after-spike currents, [11] shows that adding a refractory time increases the accuracy of their model in reproducing biological spike data. Another biophysical parameter that could be implemented is an adaptive threshold; while heterogeneity introduces variance in the thresholds between neurons, each neuron is currently associated with a specific threshold. This is handled in [11] by introducing a subthreshold voltage component to the threshold value, which depends on both the reset and current voltage; while this has little impact on the accuracy of representing inhibitory firings, it shows an increase in the model's ability to represent biologically accurate excitatory spikes.

§4.3: Final Thoughts

In this thesis we explain the basic biophysical properties of neurons and how these could be modeled in various ways. We point out a biologically relevant problem in the form of seizure, and more specifically epilepsy, with discussion of how this disorder could be modelled. We introduce a leaky integrate-and-fire model which includes neural coupling and search for parameters which lead to regimes where shifts in synchrony are likely, as this is representative of a brain region which is prone to seizure. Once the fundamental properties of this regime are found, we introduce an oscillatory input, which we use to represent a nearby neural region undergoing its own seizure; while this is our justification for an oscillatory input, the reasoning could be extended to anything from auditory waves to the common idea of flashing lights at a given frequency. With a functioning

model that lies in a regime prone to shifts in synchrony, where it experiences input oscillations indicative of a nearby microseizure, we investigate heterogeneity and its interaction with neural firing. We find results that agree with biological data, specifically that heterogeneity decorrelates the system and makes it resistant to undergoing seizure-like behaviour, in part due to a suppression of harmonics. We also find that heterogeneity suppresses resonant frequencies and linearizes the system, aiding in the decorrelation of neural firing.

Appendix:

Fourier Transform

All information regarding Fourier transforms in this section is taken from [5].

Fourier series express a periodic function as a sum of sine and cosine functions; while Fourier series apply to periodic functions the Fourier transform applies to all functions by making them periodic over an infinite interval, which is equivalent to a function not being periodic. The general Fourier transform takes the form:

$$f(x) = \int_{-\infty}^{\infty} g(a)e^{iax}da$$

with its inverse Fourier transform taking the form:

$$g(a) = \frac{1}{2\pi}\int_{-\infty}^{\infty} f(x)e^{-iax}dx$$

As evident from these equations, the Fourier transform converts a function of one variable (*g(a)*) to a function of another (*f(x)*). We use the Fourier transform to convert our firing rate, which is a function of time, to the power spectra, which is a function of frequency.

Coding Specifics

All code was written and compiled in Python 3 by Paul Anthony Foley.

Code was primarily written using the following versions:

Numpy: 1.19.2

Matplotlib: 3.3.2

Python: 3.8.5

While updates were used for certain code, that version cannot be verified due to the computer no longer being in my possession.

While most of the code follows the LIF model proposed in this thesis, and uses the Euler method to solve the associated differential equation, there are a few properties not previously discussed.

1) Gaussian white noise is proportional to $\sqrt{dt}$ rather than the standard *dt*. This is due to statistical properties.
2) The impact of synaptic weights are time-independent, and thus do not grow with *dt*. This is standard in computational neuroscience.
3) The base code was written to be extremely flexible, and as such contains many unused variables. An example of this is the time since spike – *tss* – which is implemented for refractory times but is not used.
4) Multiline comments are used often to remove large portions of code, and follow the form #''' CODE #'''. If handling this, only the initial # has to be removed/added to remove the chunk of code.

Example code is found at:

https://github.com/Foelley/PAFLIFMscThesis/blob/main/PAFLIFMscThesis

While specific values change according to what was investigated, or were placed in multidimensional loops, this is the main base code that would be altered.

References:

[1]: Dayan, P., & Abbott, L. (2014). *Theoretical neuroscience: Computational and mathematical modeling of neural systems*. MIT Press.

[2]: Xu, Z., Wu, W., Winter, S. S., Mehlman, M. L., Butler, W. N., Simmons, C. M., Harvey, R. E., Berkowitz, L. E., Chen, Y., Taube, J. S., Wilber, A. A., & Clark, B. J. (2019). A comparison of neural decoding methods and population coding across thalamo-cortical head direction cells. *Frontiers in Neural Circuits, 13*. https://doi.org/10.3389/fncir.2019.00075

[3]: Abbott, A. (2021, October 22). Billion-Dollar Brain Maps: What We've Learnt. *Nature, 598*, 22–25.

[4]: Gerstner, W., & Kistler, W. M. (2008). *Spiking neuron models: Single neurons, populations, plasticity*. Cambridge Univ. Press.

[5]: Boas, M. L. (2015). Fourier Series and Transforms. In *Mathematical methods in the physical sciences*. essay, Wiley.

[6]: Brunel, N., Hakim, V., & Richardson, M. J. (2003). Firing-rate resonance in a generalized integrate-and-fire neuron with subthreshold resonance. *Physical Review E, 67*(5). https://doi.org/10.1103/physreve.67.051916

[7]: HODGKIN, A., & HUXLEY, A. (1990). A quantitative description of membrane current and its application to conduction and excitation in nerve. *Bulletin of Mathematical Biology, 52*(1-2), 25–71. https://doi.org/10.1016/s0092-8240(05)80004-7

[8]: Rodríguez-Collado, A., & Rueda, C. (2021). A simple parametric representation of the Hodgkin-Huxley model. *PLOS ONE, 16*(7). https://doi.org/10.1371/journal.pone.0254152

[9]: Brunel, N., & van Rossum, M. C. (2007). Lapicque's 1907 paper: From frogs to integrate-and-fire. *Biological Cybernetics, 97*(5-6), 337–339. https://doi.org/10.1007/s00422-007-0190-0

[10]: Abbott, L. F. (1999). Lapicque's introduction of the integrate-and-fire model neuron (1907). *Brain Research Bulletin, 50*(5-6), 303–304. https://doi.org/10.1016/s0361-9230(99)00161-6

[11]: Teeter, C., Iyer, R., Menon, V., Gouwens, N., Feng, D., Berg, J., Szafer, A., Cain, N., Zeng, H., Hawrylycz, M., Koch, C., & Mihalas, S. (2018). Generalized leaky integrate-and-fire models classify multiple neuron types. *Nature Communications, 9*(1). https://doi.org/10.1038/s41467-017-02717-4

[12]: Roxin, A., Brunel, N., Hansel, D., Mongillo, G., & van Vreeswijk, C. (2011). On the distribution of firing rates in networks of cortical neurons. *Journal of Neuroscience*, *31*(45), 16217–16226. https://doi.org/10.1523/jneurosci.1677-11.2011

[13]: Stein. (2000). *Digital Signal Processing a computer science perspective*. John Wiley.

[14]: Rich, S., Booth, V., & Zochowski, M. (2016). Intrinsic cellular properties and connectivity density determine variable clustering patterns in randomly connected inhibitory neural networks. *Frontiers in Neural Circuits*, *10*. https://doi.org/10.3389/fncir.2016.00082

[15]: Jiruska, P., de Curtis, M., Jefferys, J. G., Schevon, C. A., Schiff, S. J., & Schindler, K. (2013). Synchronization and desynchronization in epilepsy: Controversies and hypotheses. *The Journal of Physiology*, *591*(4), 787–797. https://doi.org/10.1113/jphysiol.2012.239590

[16]: Rich, S., Chameh, H. M., Lefebvre, J., & Valiante, T. A. (2021). Resilience through diversity: Loss of neuronal heterogeneity in epileptogenic human tissue impairs network resilience to sudden changes in synchrony. https://doi.org/10.1101/2021.03.02.433627

[17]: Gerstner, W., Kistler, W. M., Naud, R., & Paninski, L. (2016). *Neuronal dynamics from single neurons to networks and models of cognition*. Cambridge University Press.

[18]: Dutta, S., Kumar, V., Shukla, A., Mohapatra, N. R., & Ganguly, U. (2017). Leaky integrate and fire neuron by charge-discharge dynamics in floating-body MOSFET. *Scientific Reports*, *7*(1). https://doi.org/10.1038/s41598-017-07418-y

[19]: Slaughter, M. (2002). *Basic concepts in neuroscience: A student's Survival Guide ; great for course prep and Usmle*. McGraw-Hill.

[20]: Griffiths, D. J. (2019). *Introduction to electrodynamics*. Cambridge University Press.

[21]: Mehaffey, W. H., & Doupe, A. J. (2015). Naturalistic stimulation drives opposing heterosynaptic plasticity at two inputs to Songbird Cortex. *Nature Neuroscience*, *18*(9), 1272–1280. https://doi.org/10.1038/nn.4078

[22]: Rich, S., Hutt, A., Skinner, F. K., Valiante, T. A., & Lefebvre, J. (2020). Neurostimulation stabilizes spiking neural networks by disrupting seizure-like oscillatory transitions. *Scientific Reports*, *10*(1). https://doi.org/10.1038/s41598-020-72335-6

[23]: Nagaeva, E., Zubarev, I., Bengtsson Gonzales, C., Forss, M., Nikouei, K., de Miguel, E., Elsilä, L., Linden, A.-M., Hjerling-Leffler, J., Augustine, G. J., & Korpi, E. R. (2020). Heterogeneous somatostatin-expressing neuron population in mouse ventral tegmental area. *ELife*, *9*. https://doi.org/10.7554/elife.59328

[24]: Mishra, P., & Narayanan, R. (2018). Disparate forms of heterogeneities and interactions among them drive channel decorrelation in the dentate gyrus: Degeneracy and dominance. *Hippocampus*, *29*(4), 378–403. https://doi.org/10.1002/hipo.23035

[25]: Jirsa, V. K., Stacey, W. C., Quilichini, P. P., Ivanov, A. I., & Bernard, C. (2014). On the nature of seizure dynamics. *Brain*, *137*(8), 2210–2230. https://doi.org/10.1093/brain/awu133

[26]: Mejias, J. F., & Longtin, A. Ã. (2014). Differential effects of excitatory and inhibitory heterogeneity on the gain and asynchronous state of sparse cortical networks. *Frontiers in Computational Neuroscience*, *8*. https://doi.org/10.3389/fncom.2014.00107

[27]: Moran, L. V., & Hong, L. E. (2011). High vs low frequency neural oscillations in schizophrenia. *Schizophrenia Bulletin*, *37*(4), 659–663. https://doi.org/10.1093/schbul/sbr056

[28]: Lagarde, S., Bonini, F., McGonigal, A., Chauvel, P., Gavaret, M., Scavarda, D., Carron, R., Régis, J., Aubert, S., Villeneuve, N., Giusiano, B., Figarella-Branger, D., Trebuchon, A., & Bartolomei, F. (2016). Seizure-onset patterns in focal cortical dysplasia and neurodevelopmental tumors: Relationship with surgical prognosis and neuropathologic subtypes. *Epilepsia*, *57*(9), 1426–1435. https://doi.org/10.1111/epi.13464

[29]: Bienenstock, E. L., Cooper, L. N., & Munro, P. W. (1982). Theory for the development of neuron selectivity: Orientation specificity and binocular interaction in visual cortex. *The Journal of Neuroscience*, *2*(1), 32–48. https://doi.org/10.1523/jneurosci.02-01-00032.1982

[30]: Scofield, C. L., & Cooper, L. N. (1985). Development and properties of Neural Networks. *Contemporary Physics*, *26*(2), 125–145. https://doi.org/10.1080/00107518508210744

[31]: Cooper, L. N., & Scofield, C. L. (1988). Mean field theory of a neural network. https://doi.org/10.21236/ada190801

[32]: Treves, A. (1993). Mean-field analysis of neuronal Spike Dynamics. *Network: Computation in Neural Systems*, *4*(3), 259–284. https://doi.org/10.1088/0954-898x_4_3_002

[33]: Abbott, L. F., & van Vreeswijk, C. (1993). Asynchronous states in networks of pulse-coupled oscillators. *Physical Review E*, *48*(2), 1483–1490. https://doi.org/10.1103/physreve.48.1483

[34]: Brunel, N. (2000). Dynamics of networks of randomly connected excitatory and inhibitory spiking neurons. *Journal of Physiology-Paris*, *94*(5-6), 445–463. https://doi.org/10.1016/s0928-4257(00)01084-6

[35]: Mirollo, R. E., & Strogatz, S. H. (1990). Synchronization of pulse-coupled biological oscillators. *SIAM Journal on Applied Mathematics*, *50*(6), 1645–1662. https://doi.org/10.1137/0150098

[36]: Merriam-Webster. (n.d.). *Rheobase definition & meaning*. Merriam-Webster. Retrieved August 17, 2022, from https://www.merriam-webster.com/medical/rheobase

[37]: Neske, G. T., Patrick, S. L., & Connors, B. W. (2015). Contributions of diverse excitatory and inhibitory neurons to recurrent network activity in cerebral cortex. *Journal of Neuroscience*, *35*(3), 1089–1105. https://doi.org/10.1523/jneurosci.2279-14.2015

[38]: Baltus, A., & Herrmann, C. S. (2016). The importance of individual frequencies of endogenous brain oscillations for auditory cognition – A short review. *Brain Research*, *1640*, 243–250. https://doi.org/10.1016/j.brainres.2015.09.030

[39]: Lea-Carnall, C. A., Montemurro, M. A., Trujillo-Barreto, N. J., Parkes, L. M., & El-Deredy, W. (2016). Cortical resonance frequencies emerge from network size and connectivity. *PLOS Computational Biology*, *12*(2). https://doi.org/10.1371/journal.pcbi.1004740

[40]: Palanca-Castan, N., & Köppl, C. (2015). Change in the coding of interaural time difference along the tonotopic axis of the chicken nucleus laminaris. *Frontiers in Neural Circuits*, *9*. https://doi.org/10.3389/fncir.2015.00043

[41]: Mejias, J. F., & Longtin, A. (2012). Optimal heterogeneity for coding in spiking neural networks. *Physical Review Letters*, *108*(22). https://doi.org/10.1103/physrevlett.108.228102

[42]: Wilson, H. R., & Cowan, J. D. (1972). Excitatory and inhibitory interactions in localized populations of model neurons. *Biophysical Journal*, *12*(1), 1–24. https://doi.org/10.1016/s0006-3495(72)86068-5

[43]: Herrmann, C. S., Murray, M. M., Ionta, S., Hutt, A., & Lefebvre, J. (2016). Shaping intrinsic neural oscillations with periodic stimulation. *The Journal of Neuroscience*, *36*(19), 5328–5337. https://doi.org/10.1523/jneurosci.0236-16.2016

[44]: IZHIKEVICH, E. M. (2007). *Dynamical Systems in neuroscience: The geometry of excitability and bursting*. MIT Press.